IIa. General calculation (in elastic and plastic fields); experimental methods

Objekttyp: **Group**

Zeitschrift: **IABSE congress report = Rapport du congrès AIPC = IVBH Kongressbericht**

Band (Jahr): **5 (1956)**

PDF erstellt am: **22.07.2024**

II a 1

Rectangular staircases without beams

Balkenlose Treppen mit rechtwinkligen Grundriss

Escaliers rectangulaires sans poutres

Escadas rectangulares sem vigas

FERRY BORGES
Research Engineer
Laboratório Nacional de Engenharia Civil
Lisbon

1. *Introduction*

The most varied calculation methods have been adopted for the design of staircases consisting of rectangular flights and landings not supported by beams (1).

Besides the difficulties inherent in the calculations of plates, there is the further difficulty of defining the degree of support imparted to the flight and landing slabs by their intersection. The displacements of the intersection lines depend on the behaviour of the structure as prismatic.

Some results are presented of tests carried out on a plastic model and a reinforced concrete prototype. The main objective of the tests was to obtain information about the behaviour of this type of structures and so to be able to judge the calculation methods adopted.

The present case is considered to be another of the many examples demonstrating the advantages derivable from experimental studies, on both models and prototypes. In fact, the experimental methods not only supply information relative to the particular case studied, but, when suitably interpreted, furnish the necessary elements for judging the existing theories and the basis for establishing new calculation methods. This is of the greatest interest, in view of the limitations of the general theories which usually only give the solution of pratical problems when supple-

(1) Zuchsteiner, W. — «Treppen» — Beton Kalendar, Zweiter Teil, Wilhelm Ernst und Sohn, Berlin, 1953. Krysztal, A. — «The Design of Staircases» — Concrete and Constructional Engineering, Vol. XLIX, N.º 7, London, July 1954.

mented by further hypotheses. Experiment suggests these hypotheses and allows their evaluation.

It is often verified that forecasts made before tests, even when made by experienced engineers, are as a rule invalidated by the experimental results.

These remarks apply, above all, to constructions that differ from the conventional ones because, for the latter, the experience accumulated often allows perfectly satisfactory forecasts to be made. This is only natural as for these constructions the stage for comparing the calculation methods with the actual behaviour of the structure has been passed.

2. *Experimental studies*

The experimental studies undertaken were made on a model and a prototype.

The model of methyl metacrilate (perspex), fig. 1, represented a staircase of the type shown schematically in fig. 2, to a scale of 1/20.

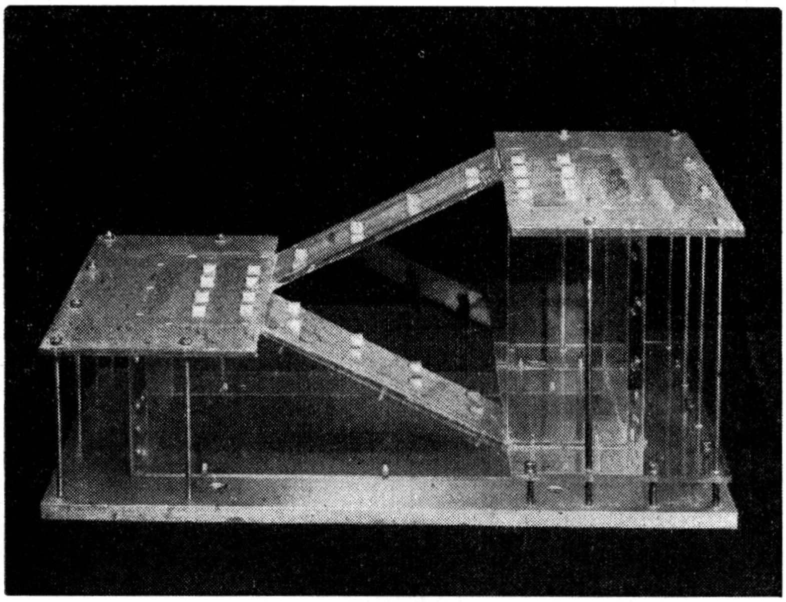

FIG. 1. Model to a scale 1/20

The numbers shown in fig. 2 indicate the dimensions of the model in centimeters. The model test consisted in the application of vertical forces and the measurements of displacements and strains at different points.

Table I gives some results obtained when applying concentrated vertical forces. Note that in spite of having sought to give a considerable horizontal rigidity to the model, this, when subject to vertical loads, underwent horizontal displacements which cannot be considered negligible.

Fig. 3 shows two of the influence surfaces of the bending moments. These surfaces were determined for 18 sections, by applying concentrated forces at different points and measuring the strains at the sections under study. Another test was carried out (fig. 4) in which a uniform load was applied. The deformation obtained is shown in fig. 5.

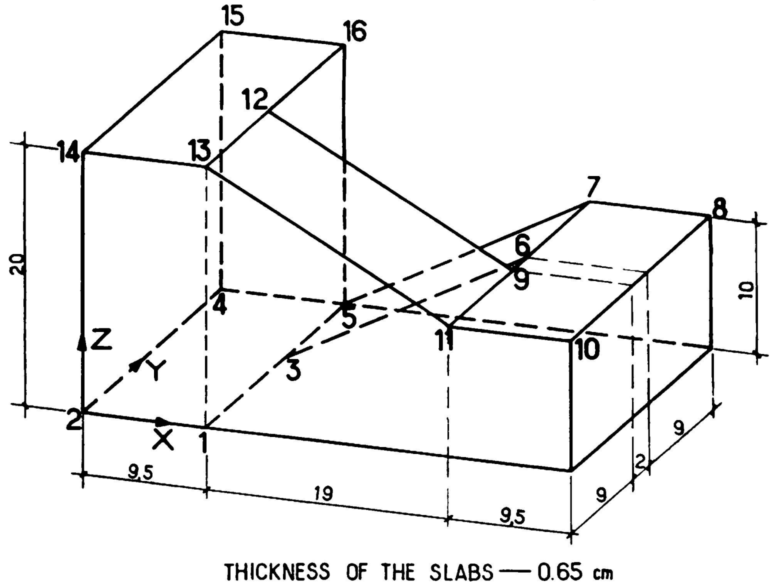

FIG. 2. Staircase studied on model

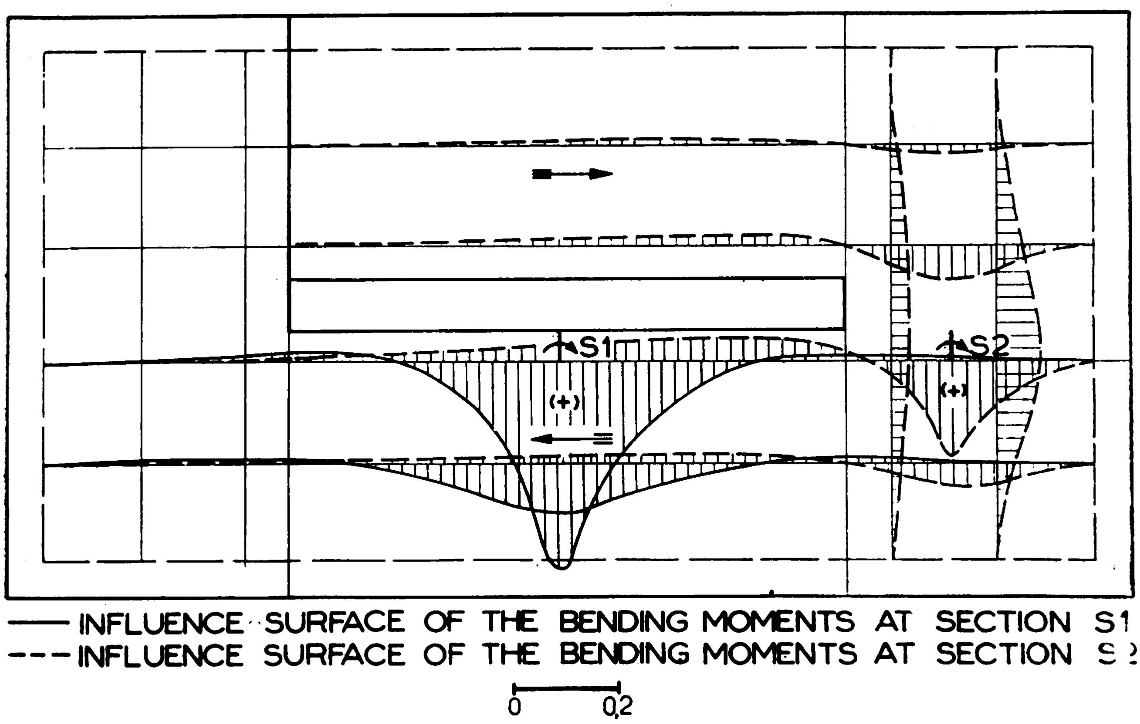

FIG. 3. Influence surfaces of the bending moments at two sections

The reinforced concrete staircase tested was of the type shown schematically in fig. 6. The landings were 20 cm thick, the flights 25 cm approximately and the rest of the dimensions are given in meters in fig. 6. As there was a guard which imparted considerable rigidity

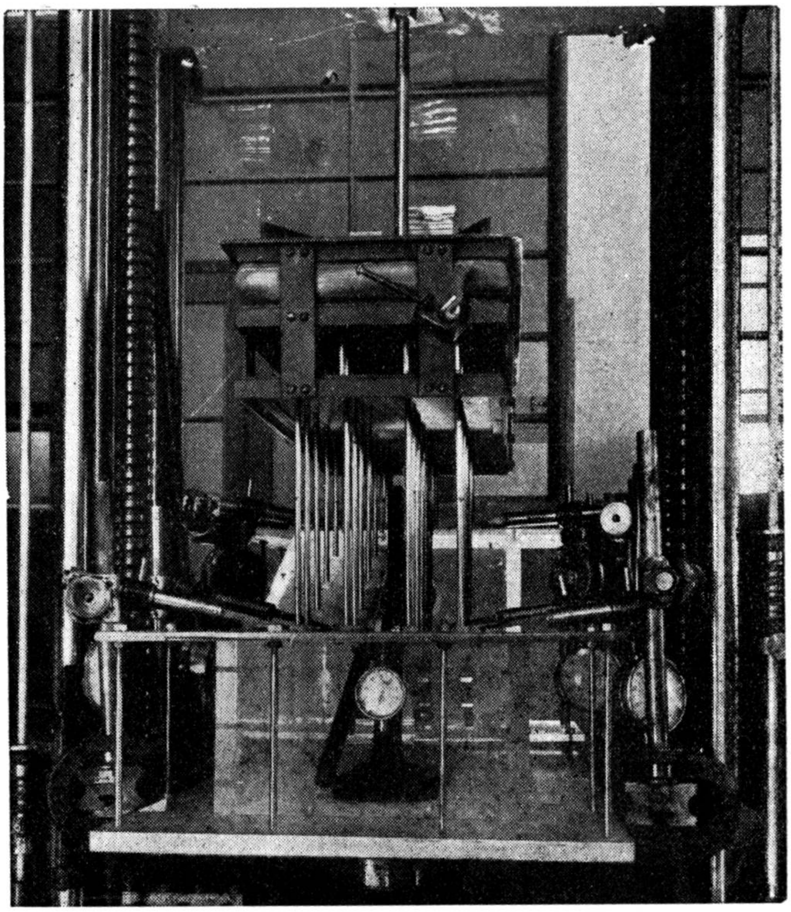

FIG. 4. Model test with uniform load

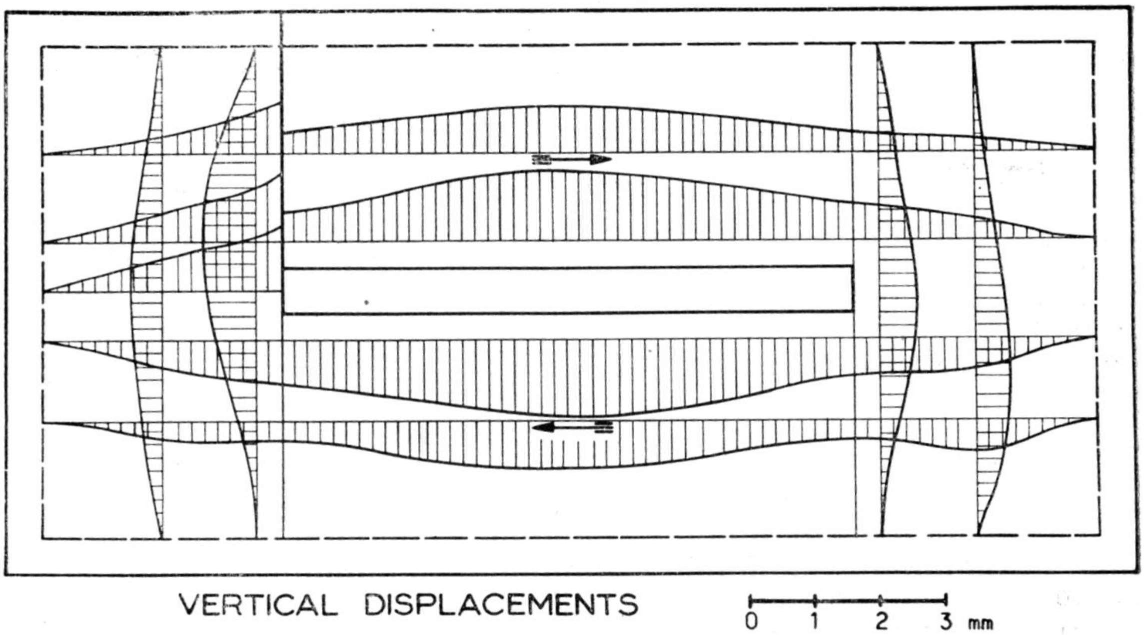

FIG. 5. Displacements due to uniform load

to the stair it was decided to make concentrated load tests before and after removal of the guard along line 17, 21 in the intermediate flight.

Fig. 7 shows the deformations obtained after removal of the guard for concentrated loads and uniform loads applied on zone (18, 19, 23, 24)

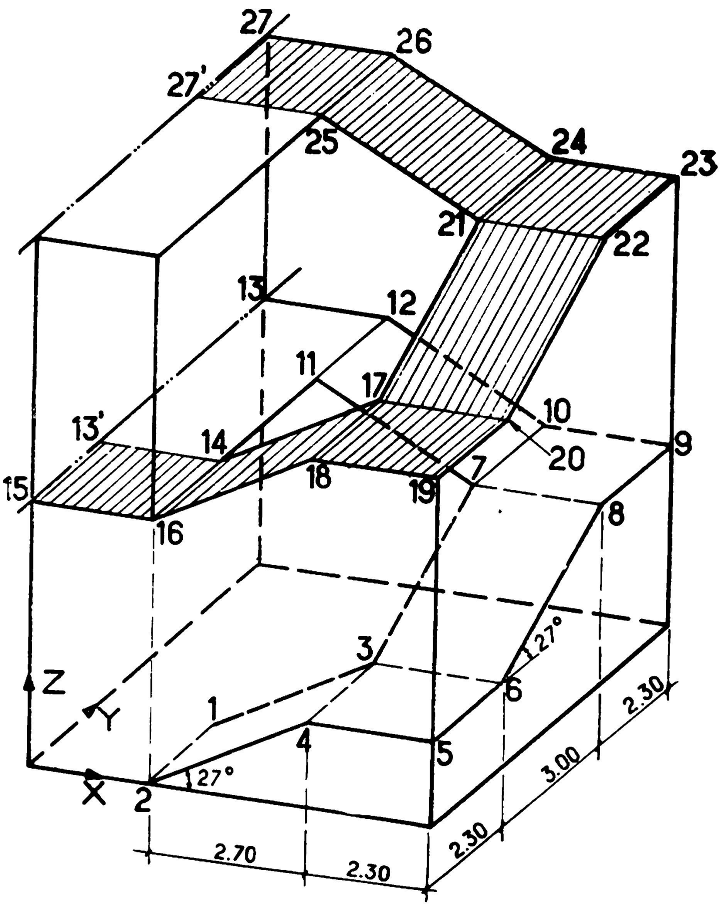

FIG. 6. Reinforced concrete staircase studied on prototype

and on the shaded zone (fig. 6). Attention is called to the considerable asymmetry of the deformations in relation to landings (17, 18, 19, 20) and (21, 22, 23, 24) which will be explained further on.

Fig. 8 gives a view of the application of the uniform load.

3. *Calculation methods*

The general theories of elastic calculation which are available cannot be applied directly to the structures concerned. The theory of plates makes it possible to study the separate behaviour of the flights or landings, but in order to be used it is necessary to know the boundary conditions which are not known, principally along the intersection lines. In fact the vertical displacements of these lines are partly impeded by the behaviour of the structure as prismatic (forces in the plane of the plates), but, the behaviour in this way imparts considerable horizontal forces which at times cannot be absorbed.

In this case, the vertical displacement of the intersection lines can increase in relation to what they would be when calculated on the basis of the structure being prismatic and assuming that supporting points in the wall cannot move horizontally.

Considering a vertical force applied to the intersection line (fig. 9), this force will resolve itself in accordance with the planes of the plates

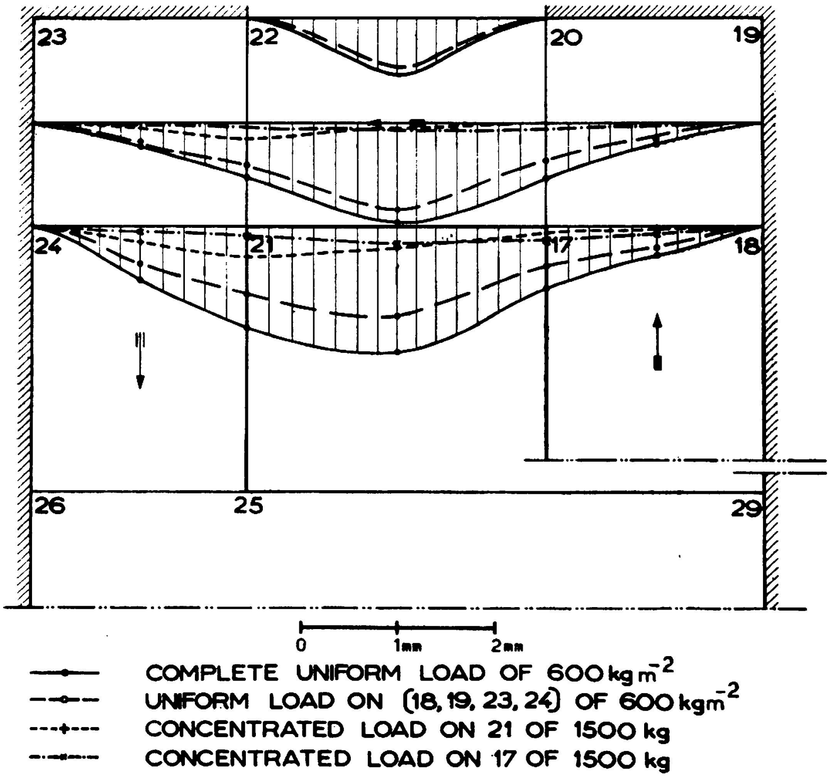

FIG. 7. Displacements measured during the test of the reinforced concrete staircase

and assuming that the points of the plates at the supports cannot undergo horizontal displacements, the vertical displacements of the intersection line can be calculated approximately from some simple hypotheses. It is considered that intersection lines remain straight and that the maximum stresses are constant along lines connecting the intersections to the supports.

Calculating, for the model of fig. 1, the displacements due to the application of a concentrated load of 10 kg at the intersection, in accordance with the above scheme, a displacement of 0.12 mm is obtained whilst the measured displacement was 0.20 mm. It is of interest to note that in the calculation the points of the other landings are assumed not to undergo deflection, which however is not borne out experimentally, as can be seen from Table I.

For the concrete staircase, the application of a concentrated load at the intersection (point 21, fig. 6), when considering the structure as prismatic, results in a calculated vertical displacement of point 21 of 0.03 mm.

The hypothesis of the structure behaving prismatically implies considerable horizontal forces, and whenever the structure cannot absorb these forces, horizontal displacements take place, which result in considerable vertical displacements of the intersection lines. Thus for example in the case of the landing (21, 22, 23, 24) of the staircase of fig. 6 when applying a vertical force in 21, forces are developed having horizontal components which tend to impose horizontal displacements of the supports corresponding to a clockwise rotation of the landing slab. These horizontal displacements result in vertical displacements of the intersections. In order to calculate these last displacements the scheme given in fig. 10 can be taken and torsional rigidity and bending moments due to the connection to the wall can be ignored, only taking into consideration the bending in a vertical plane.

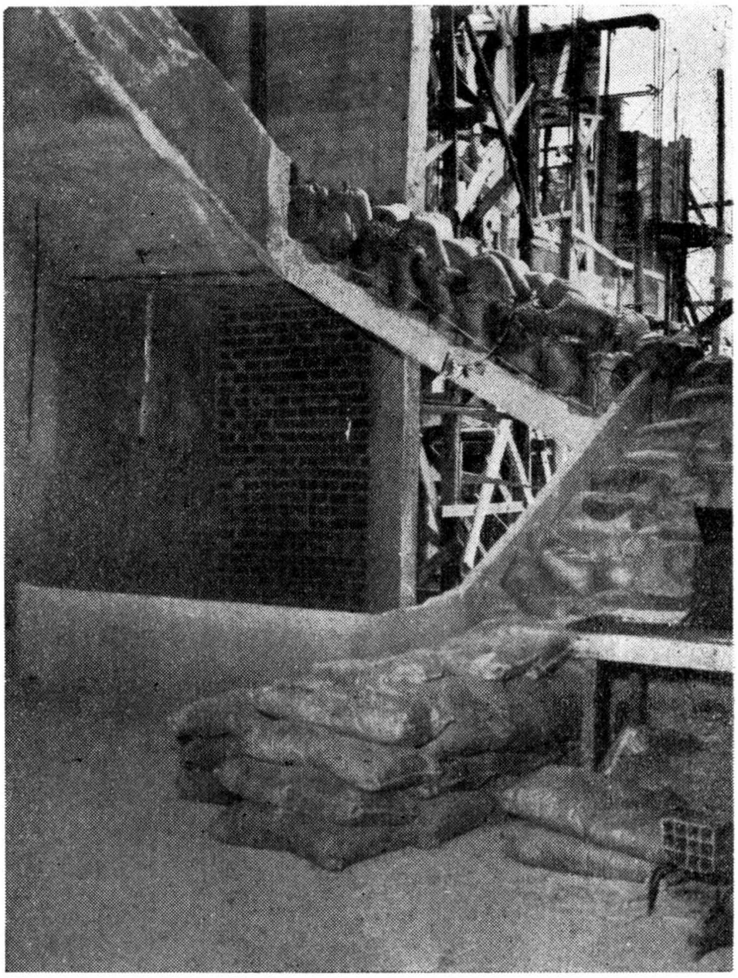

FIG. 8. Application of the uniform load

When the calculation is made in this way for a concentrated load of 1500 kg a vertical displacement of 0.40 mm was obtained, which is near the measured displacement of 0.31 mm, and much greater than the displacements computed when the structure is considered prismatic and joined to fixed points (0.03 mm).

The fact of the displacements of landing (17, 18, 19, 20) being much less than those of landing (21, 22, 23, 24) is explained by its rigid connection to the body of the building.

The above results show that it is very diffficult to obtain a horizontal rigidity which would give vertical displacements of the intersections equal to those calculated when taking the structure as prismatic.

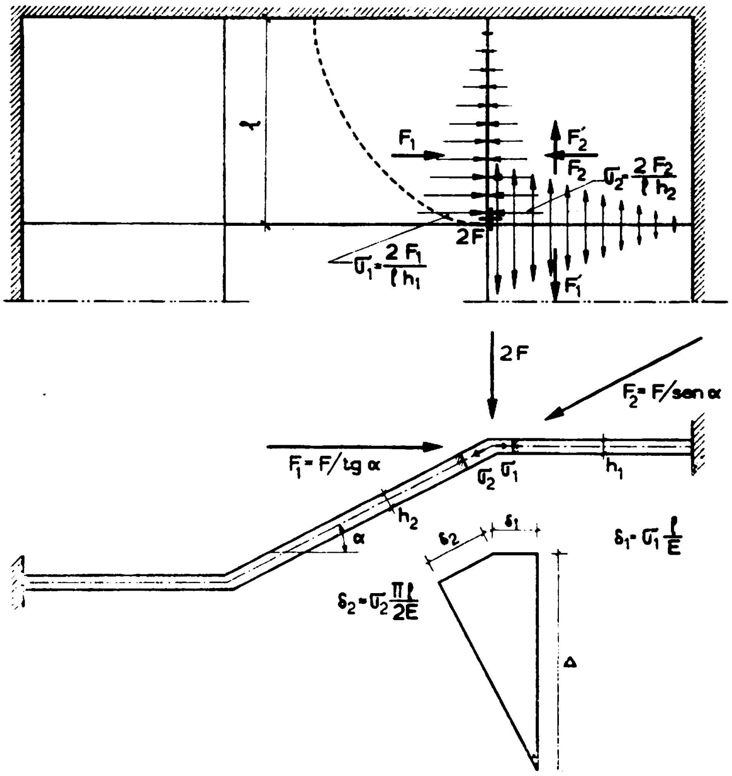

FIG. 9. Displacements of the prismatic structure

Even so, when the deformability of the staircase is small for the horizontal forces, the vertical displacements of the intersection lines between flights and landings are also small, and it would be justifiable to assume that these intersection lines function as indeformable supports in relation to the deformability of the slabs under bending. Such a hypothesis favours safety for negative bending moments at the intersections but is unfavourable for safety for positive bending moments in the middle of the flights.

When the deformability of the intersection lines is large, due to possible horizontal displacements, it becomes necessary to estimate this deformability and take it into consideration when designing the slabs. Note, for example, that in the case of the staircase of fig. 6, in spite of the important deformability of the intersections, they contribute considerably towards reducing the positive bending moments in the flights.

4. *Conclusions*

The above considerations show that the difficulty of designing staircases without beams derives from the interaction of three types

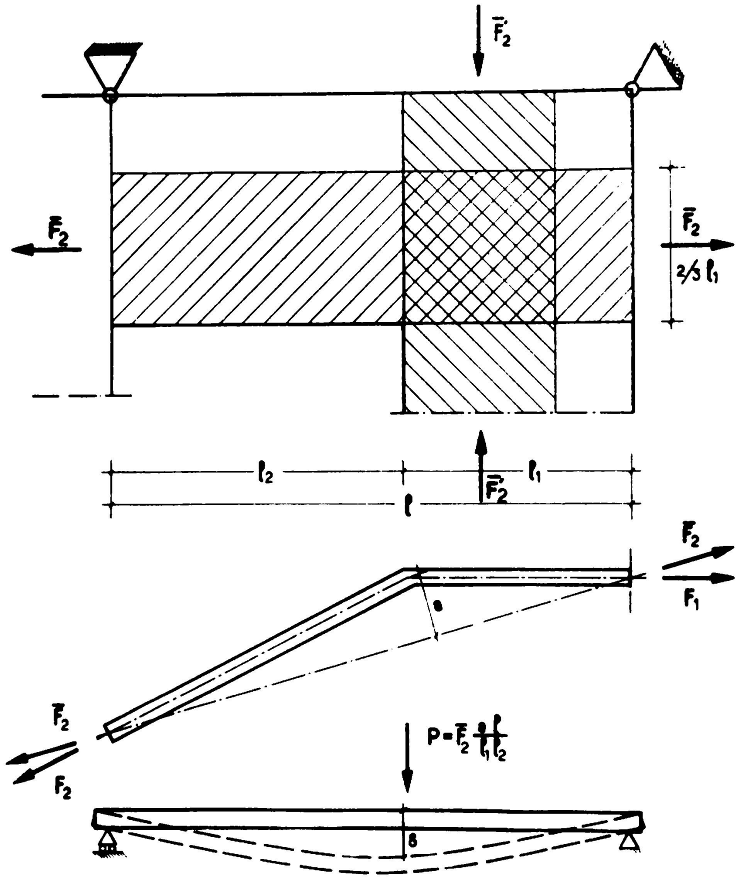

FIG. 10. Influence of horizontal displacements

of behaviour; as a plate, as a prismatic structure and in bending under the action of horizontal impulses acting on the flight and landing slabs.

In order to solve the problem it is of interest, above all, to determine the vertical deformability of the intersections, as once this is known, the problem can be solved with satisfactory approximation. This deformability depends not only on the geometry of the structure itself but also on the rigidity of the structure to which it is connected.

The considerations given are based on the criteria of elastic calculation. It is considered to be of interest also for this type of structure to develop methods of limit design.

In the case of the deformability of the intersection being small in relation to the deformability of the slabs, it should be possible to adopt a limit design for the latter assuming that the intersections behave as fixed supports. However, the value of such a method can only be proved by experiments planned for this purpose but which it has not been possible to carry out.

The author wishes to acknowledge the colaboration given by Mr. Arga e Lima in the studies related to this paper and by Mrs. Maria Emília Campos e Matos and Mr. João Madeira Costa who carried out the model and prototype tests respectively.

TABLE I

Forces		Displacements		
Point of application	Value kg	Point	Direction	Value mm
12	10	12	z z	— 0.20
		13	x x	+ 0.01
		16	x x	— 0.03
		9	z z	— 0.07
6 and 9	10	6 and 9	z z	— 0.21
		13	x x	+ 0.03
		16	x x	— 0.02
		12	z z	— 0.09
		3	z z	— 0.05
3	10	3	z z	— 0.10
		6	z z	— 0.03

SUMMARY

The results of model and prototype tests on rectangular staircases composed of slabs without beams are presented.

Design methods of this type of stairs are discussed. Such discussion is based on the interpretation of the experimental results. It is shown that to solve the problem it is especially important to determine the vertical deformability of the intersection line of the flight and landing slabs.

ZUSAMMENFASSUNG

Die vorliegende Arbeit enthält die Ergebnisse der Modell- und Prototypversuche an Treppen rechtwinkligen Grundrisses, bestehend aus nicht von Balken getragenen Platten. Auf Grund dieser Daten werden Verfahren besprochen welche zur Bemessung von Bauwerken dieser Bauart angewendet werden.

Dabei zeigt es sich, dass es besonders darauf ankommt, die lotrechte Verformung der Schnittlinien der Treppenläufe und -podeste festzustellen.

RESUMO

Apresentam-se os resultados de ensaios sobre modelo e sobre protótipo de escadas de planta rectangular constituídas por lages não apoiadas em vigas.

Discutem-se, a partir da interpretação dos resultados experimentais, os métodos de cálculo de estruturas deste tipo. Mostra-se que para resolver o problema interessa sobretudo determinar a deformabilidade vertical das linhas de intersecção entre as lages dos patins e dos lances.

RÉSUMÉ

On présente les résultats d'essais sur modèle et sur prototype d'escaliers, rectangulaires en plan, constitués par des dalles non appuyées sur des poutres.

Les méthodes de calcul de ce type d'escalier sont discutées en se fondant sur l'interprétation des résultats expérimentaux. On montre que, pour résoudre le problème, il importe surtout de déterminer la déformabilité verticale des lignes d'intersection des dalles des paliers avec celles des volées.

Leere Seite
Blank page
Page vide

II a 2

Design of shells based on the experimental determination of funicular surfaces

Schalenbemessung durch experimentelle Darstellung der Seilflächen

Dimensionamento das cúpulas a partir do traçado experimental das superfícies funiculares

Dimensionnement des coupoles minces d'après le tracé experimental des surfaces funiculaires

J. F. LOBO FIALHO
Lisbon

1 – *Introduction*

In the structural theory of shells, membrane equilibrium is defined as an abstraction of the static equilibrium of a shell obtained exclusively by means of forces contained on a plane tangent in every point to its middle surface, that is, by means of normal forces (compressive and tensile) and shear forces.

Let λ and μ denote two parameters by means of which the position of a point P on the surface of a membrane can be defined so that the equations $\lambda =$ const. and $\mu =$ const. are two families of lines on the surface (Gauss).

The square of the line element is expressed by

$$ds^2 = \alpha^2 \, d\lambda^2 + \beta^2 \, d\mu^2 = ds_1^2 + ds_2^2 \qquad (1)$$

where $\alpha = \alpha(\lambda, \mu)$ and $\beta = \beta(\lambda, \mu)$.

The equations of equilibrium of a surface element of sides ds_1, ds_2, ds_3, ds_4, are obtained by making equal to zero the forces and moments acting on the element considered.

It is established in the Differential Geometry [1] that:

$$
\begin{aligned}
ds_1 &= \beta \, d\mu \\
ds_2 &= \alpha \, d\lambda \\
ds_3 &= \left(\beta + \frac{\partial \beta}{\partial \lambda} d\lambda\right) d\mu \\
ds_4 &= \left(\alpha + \frac{\partial \alpha}{\partial \mu} d\mu\right) d\lambda
\end{aligned} \tag{2}
$$

Hence angles θ and φ (fig. 1) are:

$$
\begin{aligned}
\theta &= \frac{ds_2 - ds_4}{ds_1} = -\frac{1}{\beta} \frac{\partial \alpha}{\partial \mu} d\lambda \\
\varphi &= \frac{ds_3 - ds_1}{ds_2} = \frac{1}{\alpha} \frac{\partial \beta}{\partial \lambda} d\mu
\end{aligned} \tag{3}
$$

With the same stress notations as in the theory of plates [2] the internal forces on the edges of the element N_λ, N_μ and $N_{\lambda\mu}$ are in equilibrium with the external forces of components P_x, P_y and P_z per unit of area. Resolution of the forces in the directions of the line element ds_2 yields:

$$
-N_\lambda \beta \, d\mu + N_\lambda \beta \, d\mu + \frac{\partial (N_\lambda \beta)}{\partial \lambda} d\lambda \, d\mu - N_{\lambda\mu} \alpha \, d\lambda + N_{\lambda\mu} \alpha \, d\lambda
$$

$$
+ \frac{\partial (N_{\lambda\mu} \alpha)}{\partial \mu} \partial\lambda \, \partial\mu - N_{\lambda\mu} \theta \beta \, d\mu - N_\mu \varphi \alpha \, d\lambda + P_x \alpha \beta \, d\lambda \, d\mu = 0
$$

since the area of the element can be taken to be $\alpha \beta \, d\lambda \, d\mu$.

A similar equation is obtained for the equilibrium of forces in the direction of the line element ds_1. Elimination of θ and φ by means of equations (3) and simplification of results, yields the equations for shear forces:

$$
\left\{
\begin{aligned}
&\beta \frac{\partial N_\lambda}{\partial \lambda} + \alpha \frac{\partial N_{\lambda\mu}}{\partial \mu} + N_\lambda \frac{\partial \beta}{\partial \lambda} + 2 N_{\lambda\mu} \frac{\partial \alpha}{\partial \mu} - N_\mu \frac{\partial \beta}{\partial \lambda} + \alpha\beta P_x = 0 \\
&\beta \frac{\partial N_{\lambda\mu}}{\partial \lambda} + \alpha \frac{\partial N_\mu}{\partial \mu} - N_\lambda \frac{\partial \alpha}{\partial \mu} + 2 N_{\lambda\mu} \frac{\partial \beta}{\partial \lambda} + N_\mu \frac{\partial \alpha}{\partial \mu} + \alpha\beta P_y = 0
\end{aligned}
\right. \tag{4}
$$

---

[1] W. C. Graustein — «Differential Geometry» — The Macmillan Company, New York, NY 1935.
[2] Timoshenko — Theory of Plates and Shells—Mc Graw-Hill Book Company, Inc. New York, 1940.

Let R_I and R_{II} be the principal radii of curvature of the surface and OXYZ a rectangular system of co-ordinates connected to each point of the membrane so that OZ has the direction of the normal to the lines of principal curvature λ_o, μ_o, Fig. 2.

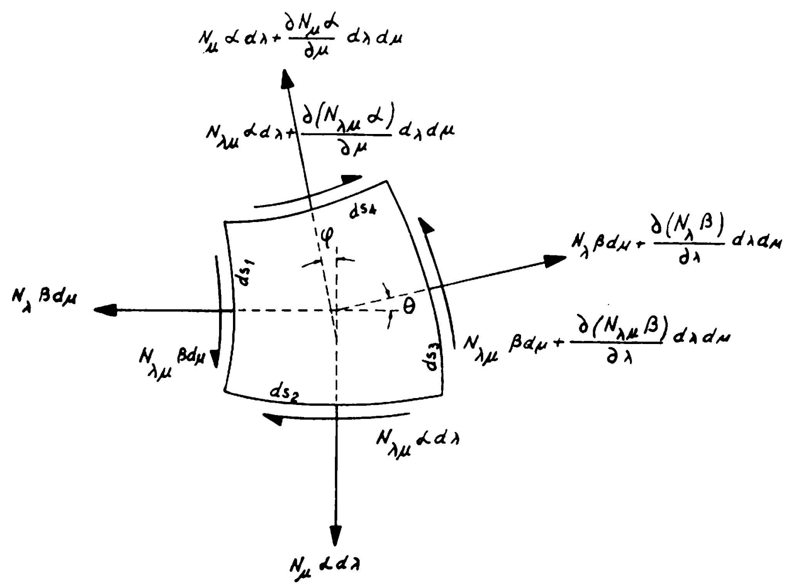

FIG. 1. Membrane equilibrium

The equilibrium equation in the direction of the normal to the surface at the point takes the following well-known form:

$$\frac{N_{\lambda_o}}{R_I} + \frac{N_{\mu_o}}{R_{II}} = P_z \tag{5}$$

These 3 equations (4) and (5) allow to evaluate the state of stress of a thin shell whatever, under a given field of forces, as they contain but three unknowns, N_λ, N_μ and $N_{\lambda\mu}$ (tensile forces).

2 – *Funicular surfaces*

It is easy to demonstrate that any structural surface can be in membrane equilibrium under a given field of forces but, as a rule this equilibrium is not funicular, i. e. the shell will be subject to compressive and tensile normal forces that will vary from point to point so as to achieve a static equilibrium between the internal shell forces and the external acting forces. In other words, this means that middle surfaces can be chosen for the shell such that under the acting field of forces, all the internal stresses will be of the same sign-all compressive or all tensile stresses. Such surfaces, called funiculars of the field of forces given, have important structural properties and are of great interest for Building Engineering.

Indeed if the middle surface of a very thin plain or slightly reinforced concrete shell is shaped as an anti-funicular surface of the acting forces a structure is obtained taking the maximum advantage of the strength of this building material. If, on the contrary, the material is steel the structural surface should receive the form of the funicular surface of the acting forces, if steel properties are to be used to the fullest.

In truth, all the builders have had this purpose intuitively in view with a more or less perfect degree of theoretical approximation,

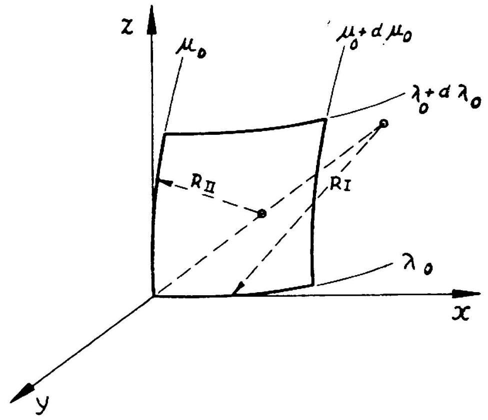

FIG. 2. Lines of curvature of a surface

what is seen in the predominant structural forms in use in all times.

Choosing at a point P a co-ordinate system λ_0, μ_0, z_0, whose z_0 — axis is normal to the shell surface and assuming the membrane to be uniformly stretched in all directions and $N_{\lambda_0} = N_{\mu_0} =$ const., the differential equation of the funicular surface may be written:

$$\left\{\begin{array}{ll} \dfrac{1}{R_I} + \dfrac{1}{R_{II}} = -\dfrac{p z_0}{\sigma d} & \text{(6a)} \\[2ex] \sigma \dfrac{\partial d}{\partial \lambda} + \alpha\, p_{\lambda_0} = 0 & \text{(6b)} \\[2ex] \sigma \dfrac{\partial d}{\partial \mu} + \beta\, p_{\mu_0} = 0 & \text{(6c)} \end{array}\right.$$

in which $p_{\lambda_0}, p_{\mu_0}, p_{z_0}$ are the components of the uniformly distributed load along the λ_0, μ_0 and z_0 axes, d the shell thickness at the point in reference and σ the constant stress in the funicular surface (tensile stresses).

$$\sigma \times d = N = \text{const.}$$

The load being uniform and hydrostatic, equations 6b and 6c disappear and taking as approximate values of the membrane curvature the second order derivatives of the deflections ξ_0 of the funicular surface in relation to the OXY plane, the following equations are obtained:

$$\begin{cases} \dfrac{1}{R_I} = -\dfrac{\partial^2 \xi}{\partial x^2} \\ \dfrac{1}{R_{II}} = -\dfrac{\partial^2 \xi}{\partial y^2} \end{cases}$$

which substituted in (6a) yield:

$$\frac{\partial^2 \xi}{\partial x^2} + \frac{\partial^2 \xi}{\partial y^2} = -\frac{p}{N} \tag{7}$$

It is thus seen that even in this particular case the determination of a funicular surface calls for the integration of Poisson's equation

$$\nabla^2 \xi = F(x, y) \tag{8}$$

Funicular surfaces have properties in respect to plates similar to those of the funicular curves in relation to beams.

Thus expressions like $\dfrac{d^4 \xi}{dx^4} = -\dfrac{p}{EI}$; $\dfrac{d^2 \xi}{dx^2} = -\dfrac{M}{EI}$ and $\dfrac{d^2 M}{dx^2} = -p$

are equivalent to $\nabla^4 \xi = -\dfrac{p}{E I_p}$; $\nabla^2 \xi = -\dfrac{M}{E I_p}$ and $\nabla^2 M = -p$ for plates,

provided that in the latter $I_p = \dfrac{e^3}{12(1-\nu^2)}$ and $M = \dfrac{m_x + m_y}{1+\nu}$.

Thus, it is seen, that as in the case of beams and arches, laws could be obtained for plates and shells connecting the shape of the funicular surface with the bending and twisting moments acting on the shell.

3 – *Search for a funicular surface by experimental means*

Scholars have always found that the search for the most adequate constant strength structural forms for certain types of acting forces is an exciting subject. Among other valuable works, mention should be made of a thesis presented at the Yugoslav Academy of Sciences in 1908 by Milankovic «Über Schalen gleicher Festigkeit». In this paper — which originated many others by other authors — Pöschl, Flugge, Forchheimer [3], etc. — it was sought to determine by analytical means the shape of some constant strength shells under acting forces with radial symmetry.

(3) Pöschl, Th.: Bauing. 8 (1927) S. 624.
Flügge, W.: Statik und Dynamik der Schalen. Berlin 1934, S. 32.
Forchheimer, Ph.: Die Berechnung ebener und gekrümmter Behälterböden. 3 Auflage. Berlin 1931, S. 23.

The differential equation of the constant strength funicular surface can be integrated in this case and the constant strength forms of radially symmetric shells and reservoirs can be obtained by analytical or graphical means.

When no radial symmetry exists for the loads or their distribution is irregular, the mathematical tool has so far been unable to solve the

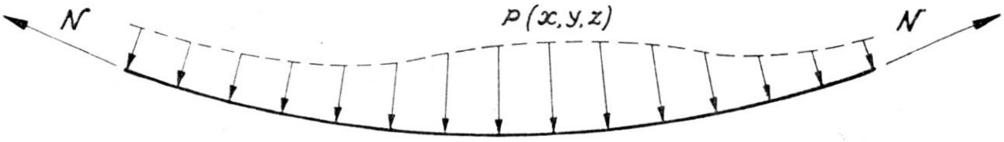

FIG. 3. Funicular equilibrium for p (x,y,z)

problem. The method we have developed half-experimental, half-analytic allows to make good this deficiency of the mathematical tools.

Consider a membrane thin and flexible enough, in tensile equilibrium under a given field of forces, fig. 3.

Obviously the shape it takes, assumed without wrinkles or folds, represents a materialization of one of the funicular surfaces of the field of forces in reference. We say one of the funicular surfaces since there is a double infinity of surfaces enjoying this property, each of them corresponding to a well-defined state of membrane equilibrium.

By a suitable variation of the membrane thickness a funicular surface of constant strength can be obtained. It suffices that the stress field in the membrane be hydrostatic and constant.

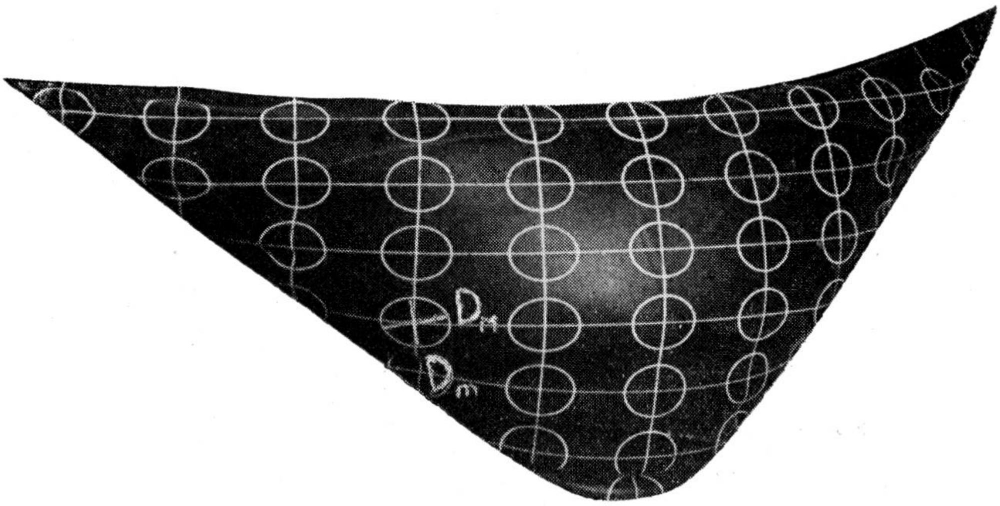

FIG. 4.

From the dimension analysis it is possible to deduce the similitude relationships between the state of stress in the elastic membrane and the state of stress in a shell whose middle surface is homologous to the model.

It is thus seen that the present method besides allowing to determine the constant strength shape of the shell surface for a given force, immediately yields the state of stress of the corresponding membrane.

4 – Experimental technique

A rubber membrane is satisfactory from this standpoint, allowing one funicular surface for a given system of forces to be very quickly obtained.

Let us suppose that on the rubber membrane that is going to be used, circumferences are drawn with diameters D_0 and center at different points. Assuming the membrane to be continuous and isotropic the circumferences of small diameter D_0 will change into elipses, the diameters of which D_m and D_M, fig. 4 and 5, will be variable from point to point both in magnitude and direction, allowing the state of stress of the membrane to be calculated. In fact let E and ν be the longitudinal modulus of elasticity and the Poisson's ratio of the membrane. Instead of defining the mean finite strains in the usual way $\varepsilon = \frac{D_m - D_0}{D_0}$, the summation of the infinitesimal strains may be used according to Hencky and Chilton [4].

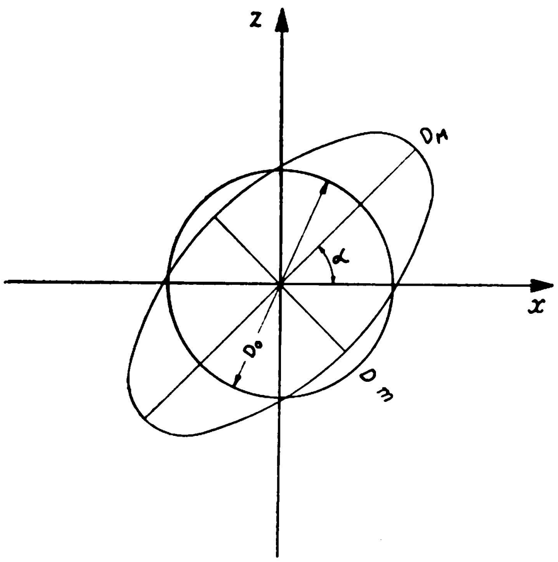

FIG. 5. Homogeneous deformation of a circle

$$\begin{aligned} \varepsilon_M &= \int_{D_0}^{D_M} d\varepsilon = \int_{D_0}^{D_M} \frac{dx}{x} = \text{Log}\frac{D_M}{D_0} \\ \varepsilon_m &= \int_{D_0}^{D_m} d\varepsilon = \int_{D_0}^{D_m} \frac{dx}{x} = \text{Log}\frac{D_m}{D_0} \end{aligned} \tag{9}$$

For strains of this magnitude and taking the deformed cross-sections of the rubber as the effective sections, Hooke's law is approximately obeyed, provided that $\varepsilon_m \leq 0.1$.

The corresponding principal stresses may be expressed by means of Hooke's law:

$$\begin{cases} \sigma_M = \dfrac{E}{1-\nu^2}(\varepsilon_M + \varepsilon_m) = \dfrac{E}{1-\nu^2}\left(\text{Log}\dfrac{D_M}{D_0} + \nu\,\text{Log}\dfrac{D_m}{D_0}\right) \\ \sigma_m = \dfrac{E}{1-\nu^2}(\varepsilon_m + \varepsilon_M) = \dfrac{E}{1-\nu^2}\left(\text{Log}\dfrac{D_m}{D_0} + \nu\,\text{Log}\dfrac{D_M}{D_0}\right) \end{cases} \tag{10}$$

[4] E. G. Chilton — Graduation Thesis at Stanford University.

These expressions hold for rubber as a first approximation, provided a certain value ε is not exceeded. However the deformation which rubber and similar substances undergo is much too large to be covered by the classical theory of small strains. An entirely new approach is required for any adequate theory of elasticity of rubber (5).

The two families of isostatics on the membrane form two orthogonal funicular nets on the surface. The stress tensor N on the membrane has at each point of the surface a maximum component given by $N_M = \sigma_M$ d, in which d represents the thickness of the deformed membrane at that point.

Once obtained the tensorial field of a funicular surface as defined by the values of N_M and N_m at any point and the two isostatics families, the state of stress of a shell with that shape can be calculated in a first approximation. Indeed, the shell having a thickness d_b and its middle surface coinciding with the funicular surface for the applied forces to a given scale $\frac{1}{\rho}$, the following expression is obtained for each point and direction:

$$\sigma = \frac{N \rho^2}{d_b} \tag{11}$$

N being the membrane stresses in the same point and direction.

It is clear that this is but an approximate value, as deformations are set up in the shell which alter its state of stress, when the field of

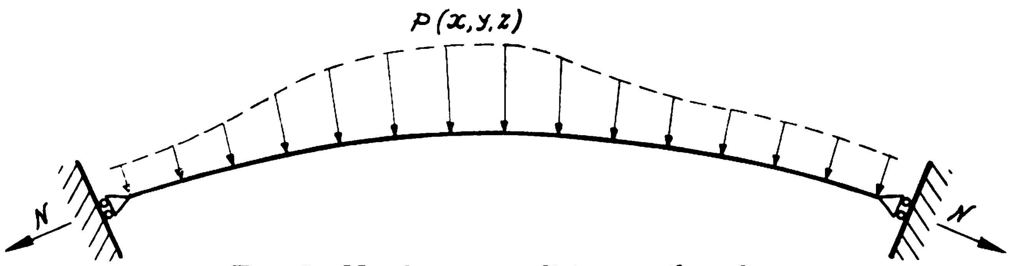

FIG. 6. Membrane condition at the edge

forces is applied. This increase of stress may be safeguarded against, by designing the shell in such a way that the membrane stresses are not much altered. The major factor disturbing the state of stress of the membrane comes from the edge conditions. For this disturbing factor to be lessened, a joint should be built allowing frictionless displacements of the edge of the shell only along a normal to the middle surface, i. e., reproducing the boundary conditions of the membrane, fig. 6. The execution of such a joint presents no technical difficulty whatsoever, improving moreover the structural behaviour of the shell and supplying more space to volumetric changes (temperature, shrinkage, etc).

(5) M. Mooney — A Theory of large elastic deformation — Journal of applied physics — Vol. 11, No. 9.

It may still be feared that this method leads to shells so thin as to make probable phenomena of buckling. The theory of the buckling of shells is still in the beginning but approximate formulas are available which give satisfatory results and connect σ_{I} and σ_{II}, the principal stresses, with the thickness of the shell, the modulus of elasticity and the Poisson's ratio of the material, and the two principal radii of curvature at each point.

5 – *Application of the method to the design of dams*

The method described in 3 was developed by the author for the study of the shape of a dam to be built in a given valley.

Indeed, dams being built in plain concrete for economic reasons, the middle surface of the structural shape adopted, should coincide with

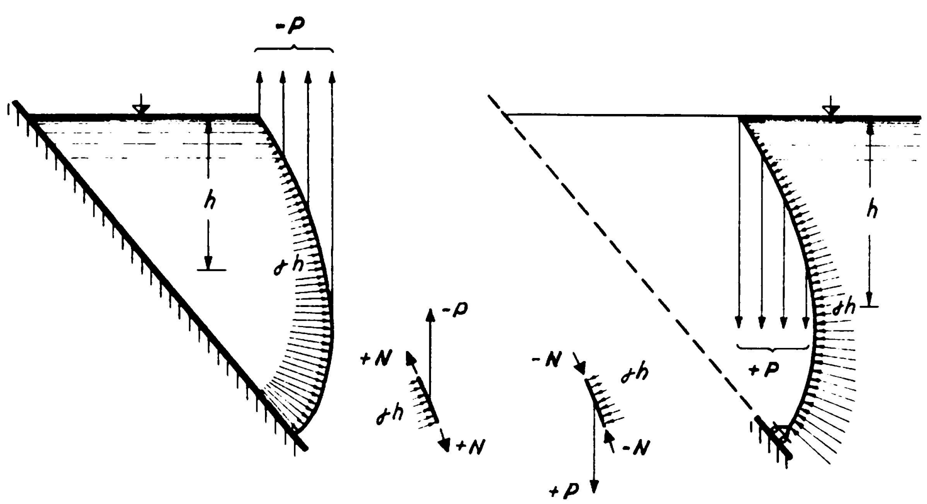

FIG. 7. Membrane equilibrium of a dam

one of the antifunicular surfaces for the forces applied. For dams, however, there are almost exclusively two importants static loads: deadweight and water pressure.

Let us consider then a rubber membrane inserted in a boundary geometrically similar to the line of contour of the valley in which the dam is to be placed. This line must be selected according to the shape and geology of the site. Be $\frac{1}{\rho}$ the scale to which this contour is reproduced. Let us take this line as the contour of a vessel for a liquid of specific gravity γ, held by a rubber membrane, fig. 7. Let us assume, additionally, that the upper contour of the membrane has no rigid connections, remaining on the free level of the fluid. Now we apply at each point of the rubber membrane a vertical load P, directed upwards, P being equal to the weight, to the scale $\frac{1}{\rho}$, of each volume element of a shell having the same middle surface but built in concrete, that is:

$$P = -2{,}4\ \gamma \frac{1}{\rho} S \qquad (12)$$

S being the area of the surface of the membrane in the center of gravity of which P acts, and d the estimated average thickness of the shell in that point.

If the shape of equilibrium displays no folds or wrinkles at any point of its surface, we may say it materializes a funicular surface for the hydrostatic pressure caused by the liquid of specific gravity γ and for the deadweight of a shell, having a middle surface with that shape, so that in each point we have:

$$\frac{N_I}{R_I} + \frac{N_{II}}{R_{II}} = \gamma z + p_n \qquad (13)$$

N_I and N_{II} being the principal membrane forces, R_I and R_{II} the two principal radii of curvature, and p_n the normal component of the deadweight. The field of membrane forces N can be evaluated by the method described in the foregoing paragraph, so that the state of stress of a dam having as middle surface the shape of the membrane under the action of the deadweight and hydrostatic pressure would be:

$$\sigma = \frac{N \rho^2}{d \gamma} \qquad (14)$$

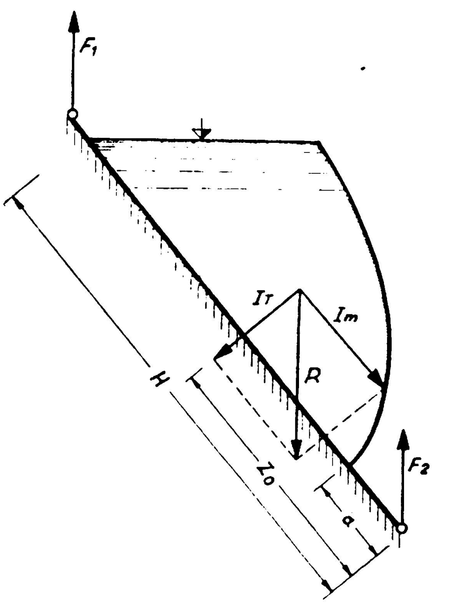

FIG. 8. Resulting vectorial equilibrium

As said above this expression holds only as a first approximation.

The following procedure, for instance, may be followed to design the dam so that the maximum stresses, as calculated by means of expression (14), do not exceed 50 kg. cm^{-2}, the increase of these stresses being checked by means of a more accurate method, e. g. three dimensional models (8) (9).

Likewise, the total hydrostatic pressure on the dam, can be evaluated by experimental means, the analytical determination being a difficult problem, owing to the shape of the upstream face.

(8) G. Oberti — *La Ricerche Sperimentale su modelli como contributo al progretto delle grandi costruzioni* — Técnica Italiana — N.° 2, 1951.

(9) M. Rocha — *General review of the present status of the experimental method of structural design.* Sep. da Publicação Preliminar do 3.° Congresso da Association Internationale des Ponts et Charpentes, Cambridge e Londres, 1952.

The hydrostatic force on the membrane is given by the following vector difference, fig. 8:

$$\vec{I_m} = \vec{R} - \vec{I_t} \tag{15}$$

R being the total weight of the container held by the membrane, which is easy to measure.

$$\vec{R} = \vec{F_1} + \vec{F_2} \tag{16}$$

The value I_t, resultant of the hydrostatic pressure on the plate is also easy to compute, provided the contour of the membrane has an easy analytical expression.

$$I_t = \int_a^H \gamma\, z\, (H - z)\, dz \tag{17}$$

The resultant I_t acts in a direction normal to the plate, at a point at a distance Z_0 from the center of application of F_2,

$$Z_0 = \frac{\int_a^H (H - z)\, z\, dz}{\int_a^H (H - z)\, dz} \tag{18}$$

Thus by means of a simple graphical construction I_m can be determined, hence the total hydrostatic pressure on the dam is:

$$\vec{I} = - I_m\, \rho^3 \tag{19}$$

6 – *Illustrative example*

In order to design a dam by the foregoing method the author devised an adequate apparatus, fig. 9. This, essentially, is made up of a plate of insertion for the membrane (1), a graduated plane to which the rubber membranes are connected by means of a hoop that materializes the insertion line. All the setup hangs from a dynamometric system (3).

A tridimensional co-ordinometer was used to measure the deformed membrane and to determine its co-ordinates referred to the system of axes OXYZ. It consists of three bars representing the three axes of the co-ordinate system, its movement being controlled by one button only (7). Before starting the test, the apparatus is set up. The plate is given the desired inclination and the position of the axes relatively to the plate is recorded by means of various adjusting screws of the co-ordinometer.

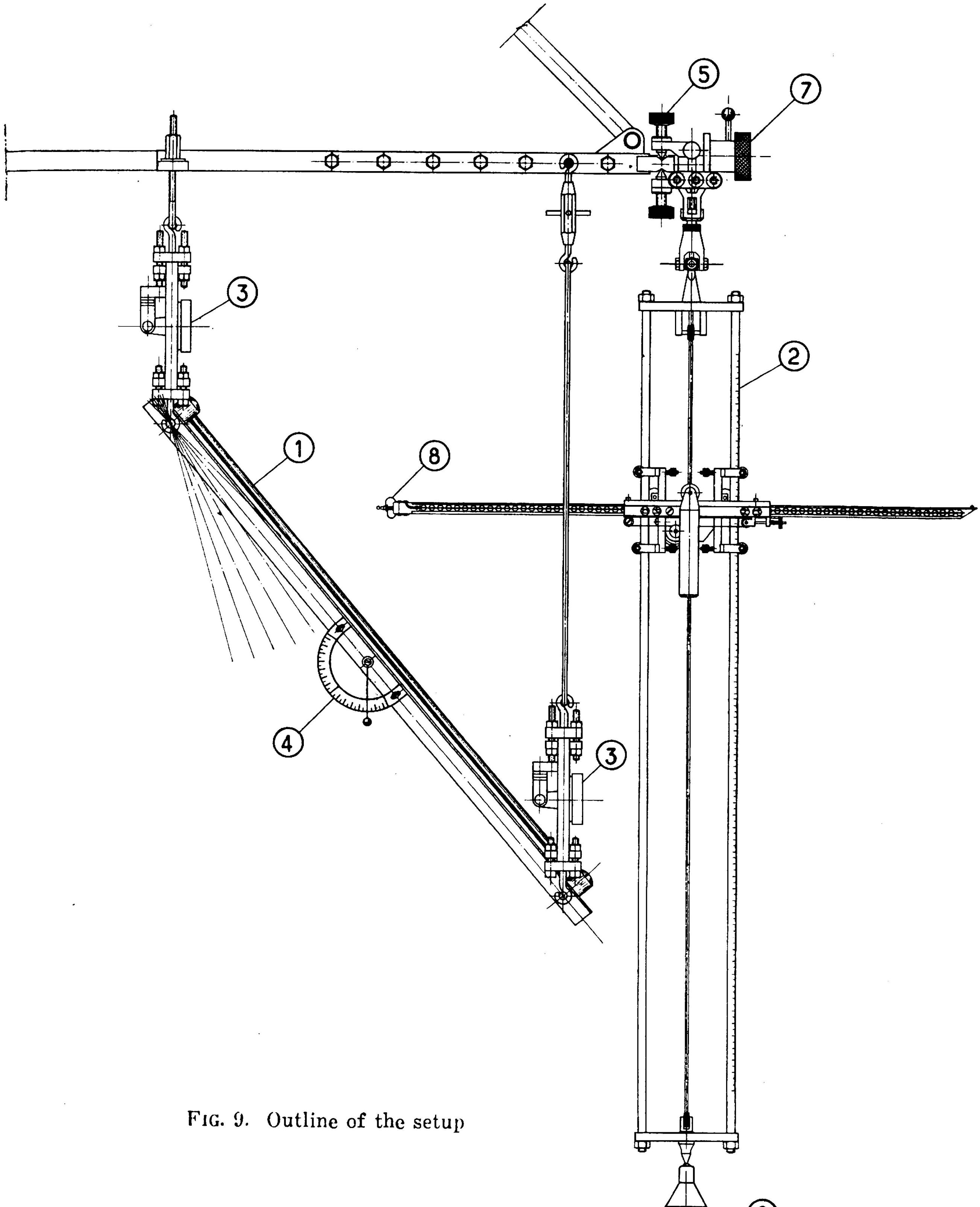

FIG. 9. Outline of the setup

The method of design, based on this experimental technique was applied to an actual case in order to check the shape and volume of a dam planned by this means [10].

The valley selected possessed an exceptional symmetry on the site of the dam, so that a symmetrical contour of simple analytical expression could be adopted.

Fig. 10 shows in full line the insertion contour adopted and in dotted line the topographic section obtained by cutting the valley by a plane.

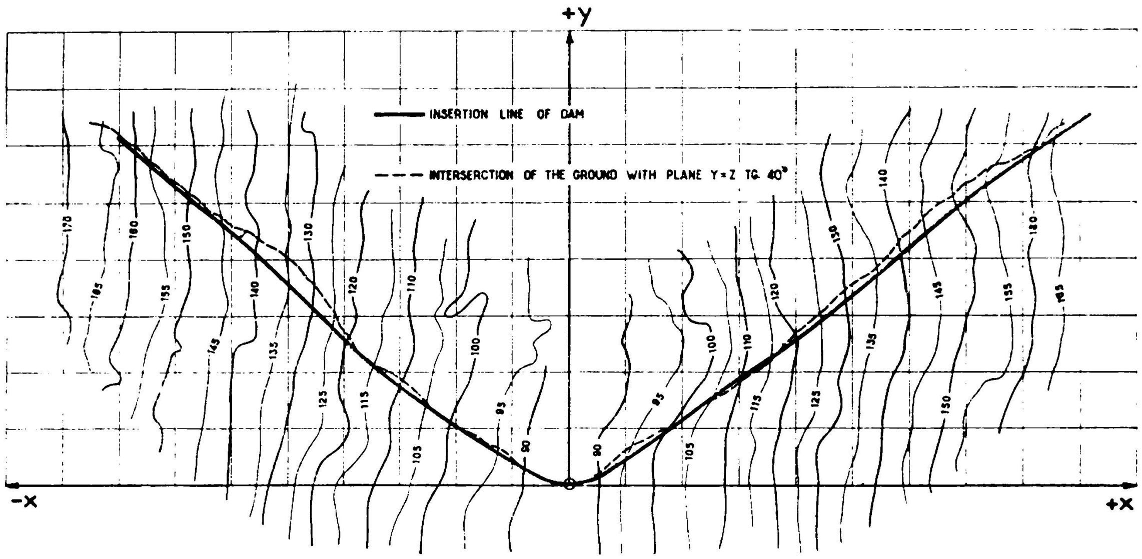

FIG. 10. Insertion lines

Relatively to the co-ordinate system OXYZ shown in the figure, in which OZ is vertical, the chosen contour is represented by the equation:

$$\begin{cases} x = \pm\sqrt{\dfrac{y\,(y+22.886)}{0,595}} \\ y = z \operatorname{tg} 40^\circ \end{cases} \qquad (20)$$

This is a branch of hyperbola resting on a plane making a 50° angle with the horizontal plane.

Pure vulcanized rubber was used to manufacture the membrane; it was calendered in both directions, in order to ensure a more perfect isotropy. The elastic properties were evaluated up to values $\varepsilon \cong 0,1$, fig. 11.

Furthermore it was sought to give such thicknesses to the membrane as to obtain surfaces of equilibrium not very different from the most recent shapes of arch dams in order to prevent constructional objections.

---

[10] The study of this dam was carried out in collaboration with Mr. Peres Rodrigues.

After some trials the shape of equilibrium shown in fig. 12 was selected. It corresponds to a distribution of thickness allowing the stress in the membrane not to exceed 50 kg. cm^{-2} as we can see in table I and fig. 13 in which the magnitudes and directions of the principal stresses were evaluated.

Afterwards the membrane was measured by means of the pendulum, and the co-ordinates in various points of the same vertical profile were determined, table II. In fig. 14 we show the horizontal curves of the deflected membrane.

The analytical definition of the dam was based on the following geometric procedure: The upstream and downstream faces were obtained

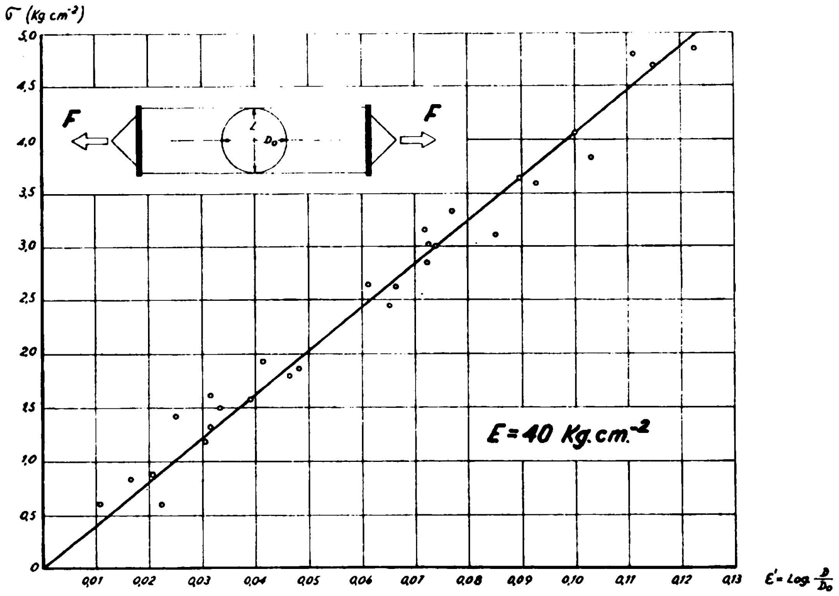

FIG. 11. Stress-strain relationship for rubber

from a middle surface, approaching as much as possible the surface of the membrane to the scale of the dam, by marking along the normal for both sides half the thickness calculated for each point.

The solid — dam — is therefore totally defined, once the equation of the middle surface and the law of the variation of thickness are settled.

The analytical definition of a middle surface as near as possible to the surface of the membrane and at the same time simple, was obtained in the following manner:

The horizontal curves are conic sections having 5 directrixes (also conics) intersecting at point (0, 0, 0). Thus the analytically defined geometric surface has no less than 17 points of contact with the surface obtained experimentally, fig. 15.

The general equation for the horizontal curves is therefore:

$$y - c - \sqrt{b - a x^2}$$

The parameters a, b, c are obtained by the condition of contact with the following directrixes:

Directrix d_e — Corresponding to the branch of hyperbola, defining the insertion line of the dam

$$\begin{cases} x_e = \pm \dfrac{y_e\,(y_e + 22{,}886)}{0{,}595} \\ y_e = z \text{ tg } 40^\circ \end{cases}$$

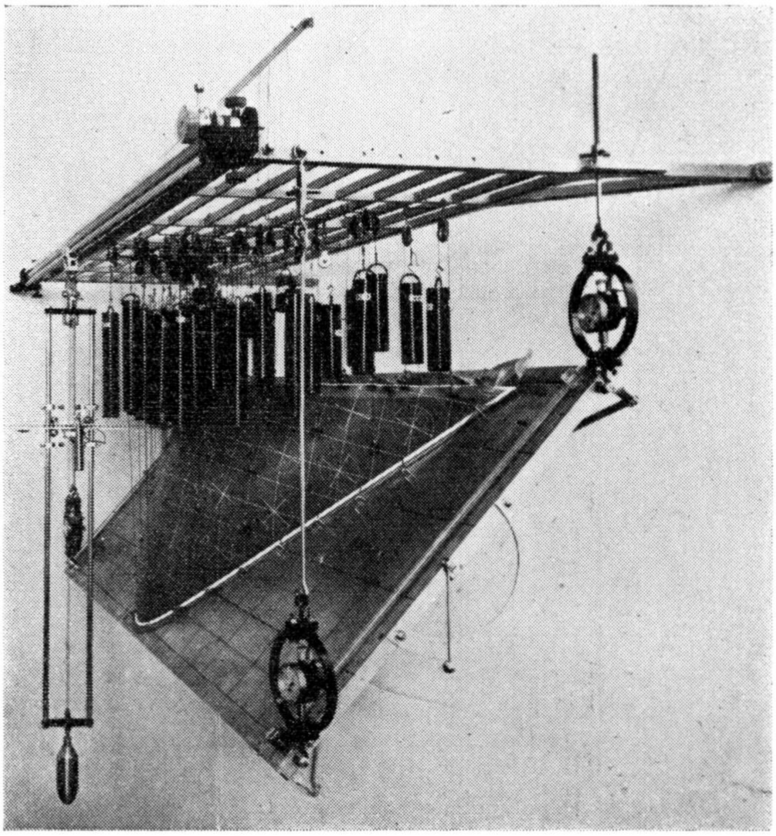

FIG. 12.

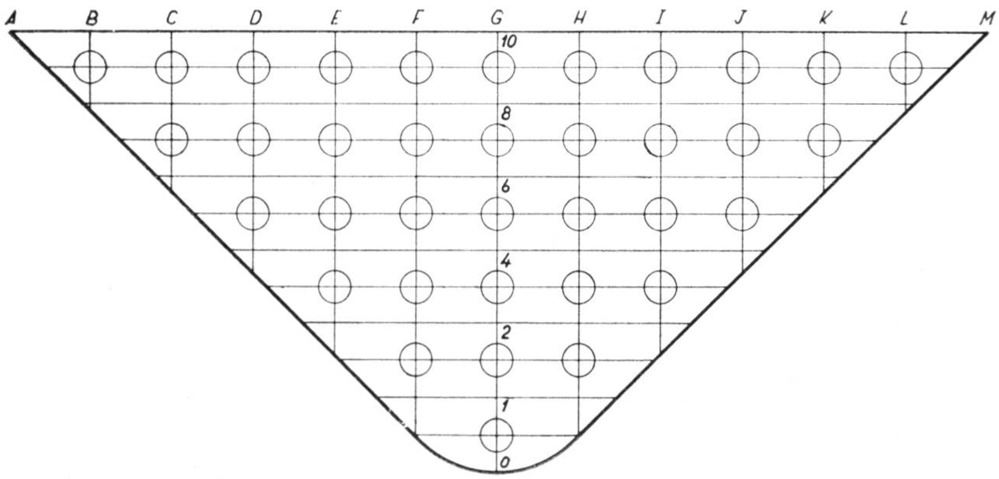

FIG. 13. Points at which the stress was measured

Directrix d_0 — Vertical profile through point (0, 0, 0)

$$\begin{cases} y_0{}^2 - (0{,}579\ Z + 24{,}240)\ y_0 + (0{,}225\ Z^2 - 5{,}7087\ Z) = 0 \\ x_0 = 0 \end{cases}$$

Directrixes d_m — Two branches of a conic section given by the expressions

$$\begin{cases} x_m{}^2 - (3{,}094\ y_m + 2{,}511)\ x_m + (5{,}587\ y_m{}^2 + 0{,}920\ y_m) = 0 \\ y_m = \dfrac{Z}{2} \end{cases}$$

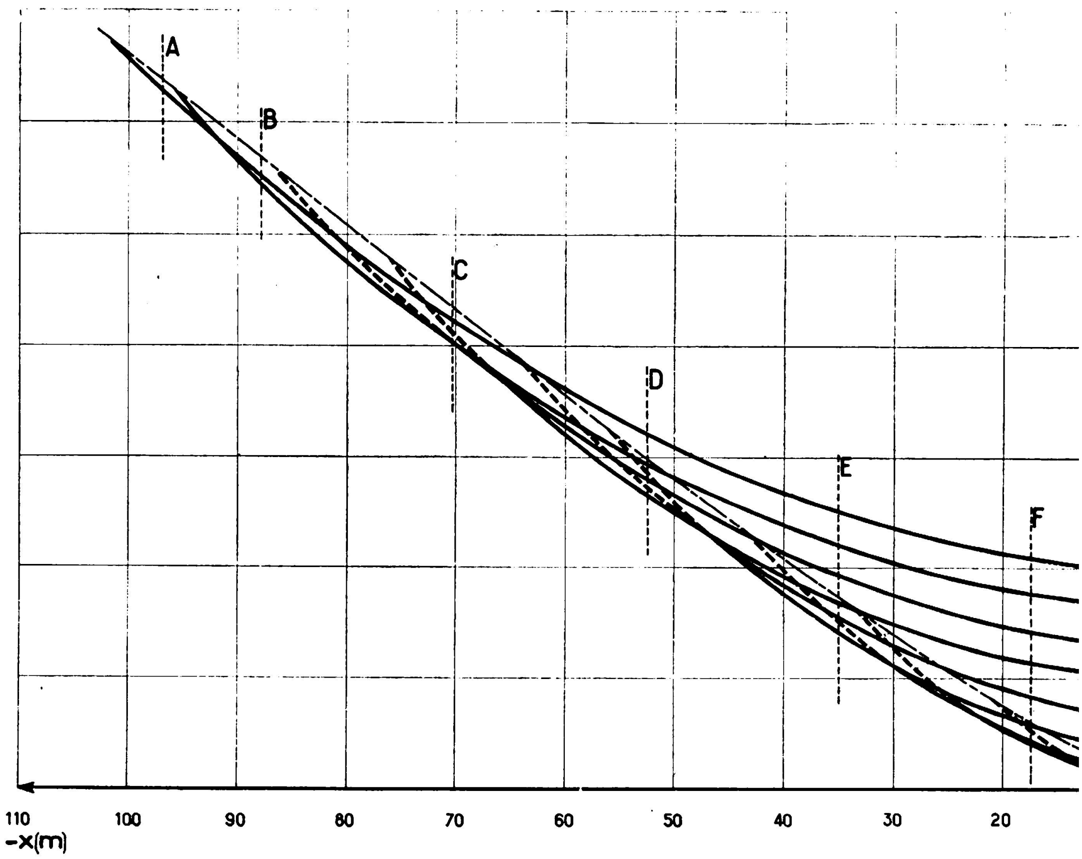

FIG. 14.

Horizontal curves of the membrane

In fig. 16 are indicated the vertical profiles of the surface, as analitically defined, and the points obtained experimentally from the co-ordinate measurements on the stretched membrane. The maximum differences do not exceed 3 mm to a scale of 1/200, that is to say they are less than 60 cm in the prototype.

The variation of the thickness of the dam was chosen in such a way, as to correspond to the loads fixed for the deadweight and, within the limits imposed by this condition, to bring about the best possible distribution of stresses inside the dam.

Thus two laws of variation for the thickness were selected according to the boundary conditions, fig. 17.

1st Case — *Built-in contour* — The thickness along the normal varies only, with respect to the elevation i. e. it does not change along a horizontal curve.

2nd Case — *Shell with a perimetric contour joint* — This joint should be made in such a way as not to disturb to a large extent the membrane conditions of the contour.

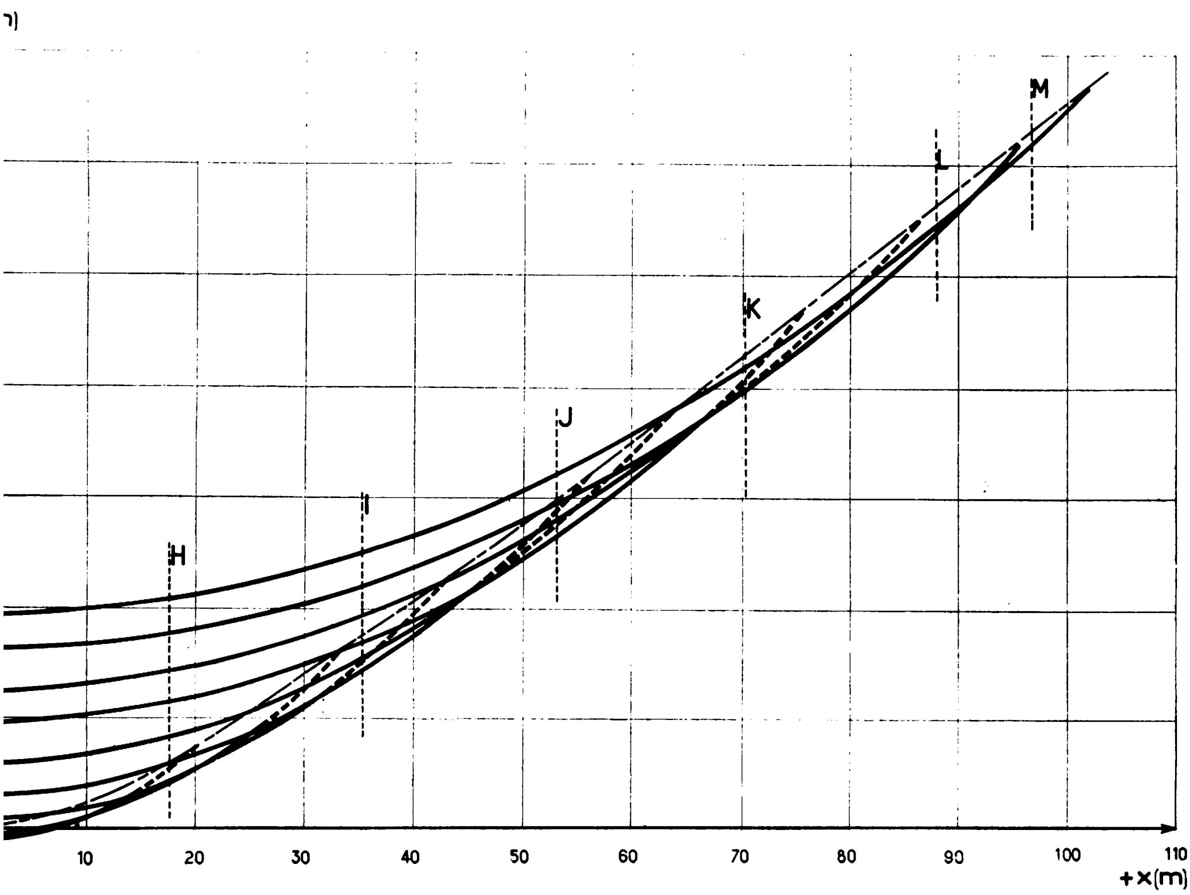

Along one horizontal curve of elevation z the thickness measured along the normal, changes according to the expression:

$$e_x = e_0 - \frac{e_0 - e_n}{d^2} x^2$$

where e_0 is the thickness of the middle cross-section as defined by the law concerning the built-in case and e_n represents the thickness

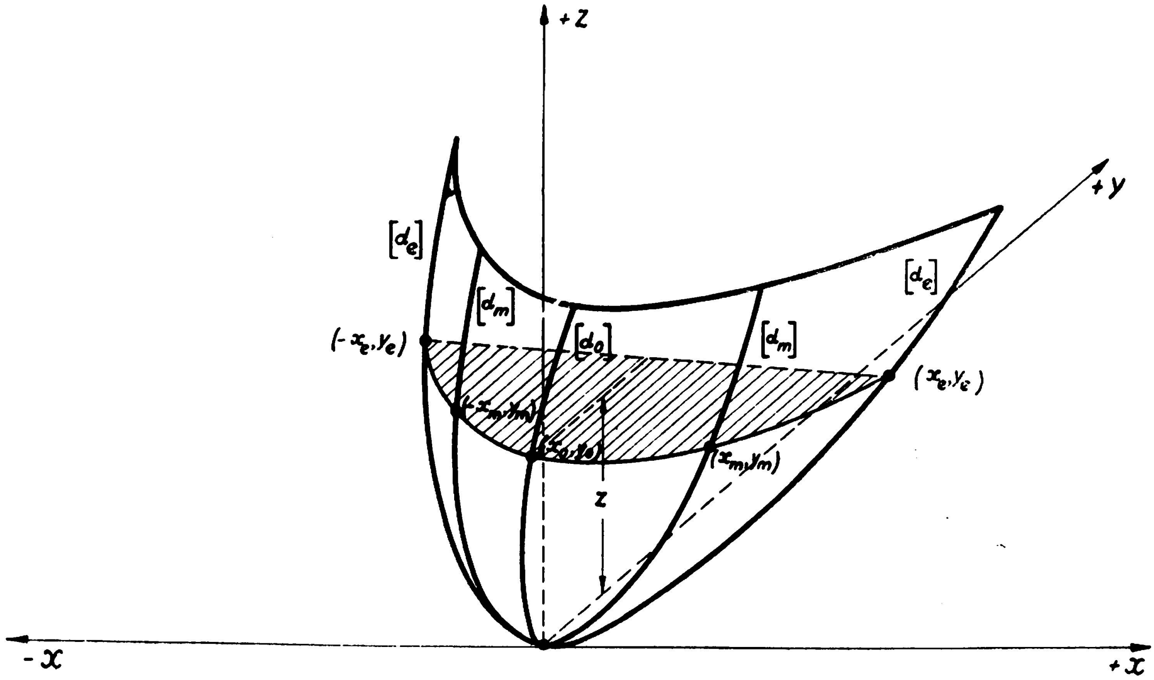

FIG. 15. Analytic expression of the middle surface

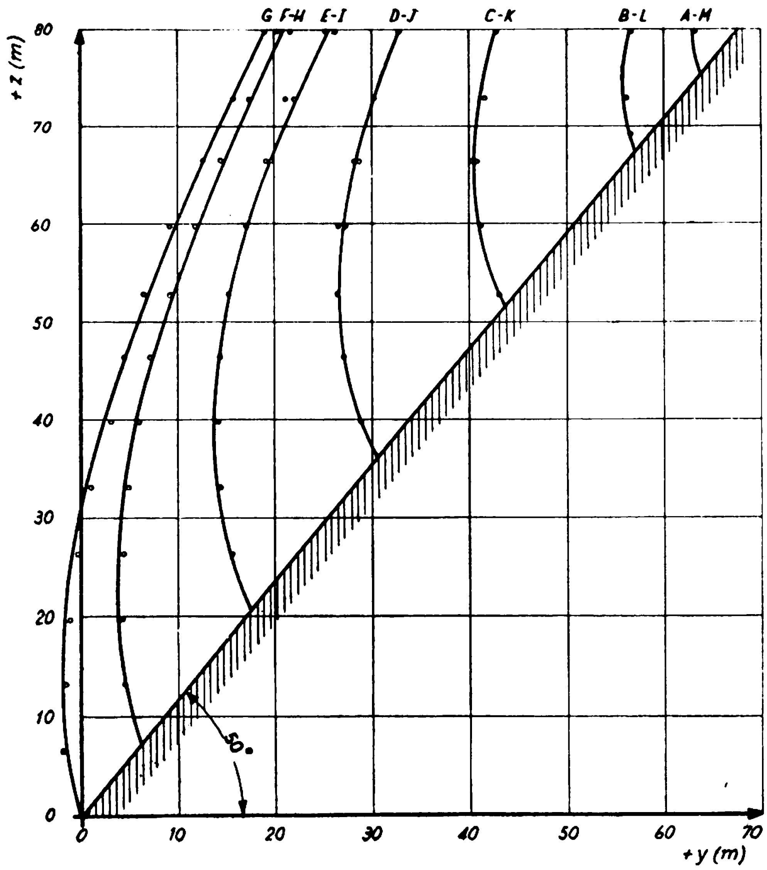

FIG. 16. Computed and experimental profiles

in the insertion contour:

$$e_n = -0{,}00146\ z^2 + 0{,}0567\ z + 6$$

d being the half-chord of the horizontal curves at that level;

$$d = \frac{z\ (z + 27{,}274)}{0{,}845}$$

That is, in this case the thickness can be somewhat smaller along the contour as the perimetral joint diminishes the moments due to the differences between the funicular surface and the middle surface, when deflected under load.

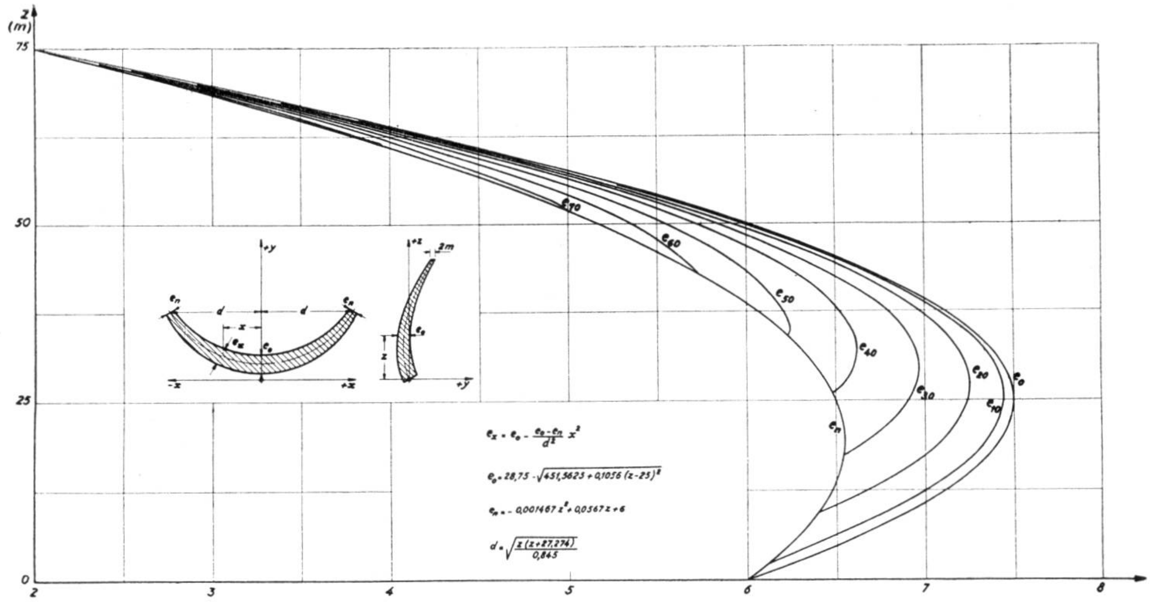

FIG. 17. Law of variation of the thickness

From these data the dam was designed with the following characteristics, fig. 18.

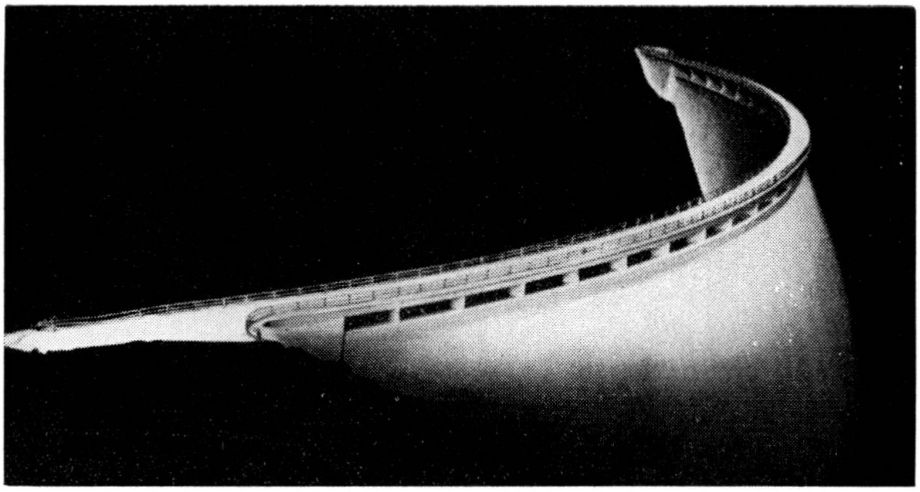

FIG. 18

Height	H = 77 m
Semi-axes of the ellipse of crest	a = 434,9 m b = 207,7 m
Angular width between the normals to the ellipse in the contour	φ = 92°
Maximum thickness of the dam	e_m = 7,5 m
Volume of concrete	V = 54 × $10^3 m^3$
Maximum length chord	C = 198 m
Maximum membrane stress (compressive)	= 46 kg. cm^{-2}

Table I

Point	Model							Prototype		
	d (mm)	ε_M (10^{-2})	ε_m (10^{-2})	σ_M (Kg cm $^{-2}$)	σ_m (Kg cm $^{-2}$)	N_M (Kg cm $^{-1}$)	N_m (Kg cm $^{-1}$)	d_b (m)	$\sigma'_b = N_M \frac{\rho^2}{d_b}$ (Kg cm $^{-2}$)	$\sigma''_b = N_m \frac{\rho^2}{d_b}$ (Kg cm $^{-2}$)
10B - 10L	0,65	3,1	-	1,3	0	0,08	0	2,00	20	0
10C - 10K	0,65	4,2	-	1,7	0	0,11	0	2,00	26	0
10D - 10J	0,65	5,6	-	2,3	0	0,15	0	2,00	35	0
10E - 10I	0,65	6,3	-	2,5	0	0,16	0	2,00	40	0
10F - 10H	0,65	6,3	-	2,5	0	0,16	0	2,00	40	0
10G	0,65	7,2	-	2,9	0	0,19	0	2,00	46	0
8C - 8K	1,10	6,4	1,3	2,6	0,3	0,29	0,03	4,10	34	4
8D - 8J	1,10	6,4	1,3	2,6	0,3	0,29	0,03	4,10	34	4
8E - 8I	1,10	7,8	1,2	3,3	0,5	0,36	0,05	4,10	42	6
8F - 8H	1,10	8,0	1,0	3,4	0,6	0,37	0,07	4,10	41	8
8G	1,10	8,6	1,0	3,7	0,7	0,40	0,08	4,10	46	9
6D - 6J	1,10	9,3	0	4,1	1,2	0,45	0,14	5,80	38	11
6E - 6I	1,10	9,4	1,0	4,0	0,9	0,44	0,09	5,80	37	8
6F - 6H	1,10	9,6	1,2	4,1	0,7	0,45	0,08	5,80	37	7
6G	1,10	9,9	1,4	4,2	0,6	0,46	0,07	5,80	38	6
4E - 4I	1,65	9,0	2,4	3,6	1,1	0,60	0,19	7,00	41	13
4F - 4H	1,65	9,0	2,4	3,6	1,1	0,60	0,19	7,00	41	13
4G	1,65	9,1	0	4,0	1,2	0,66	0,20	7,00	46	14
2F - 2H	1,65	8,0	2,0	3,2	1,2	0,54	0,20	7,00	37	14
1G	1,7	4,7	0.4	2,0	0,4	0,34	0,08	6,40	26	10

TABLE II

Profiles / Horizontal curves	y = f (x,z) (mm)						
	A — M	B — L	C — K	D — J	E — I	F — H	G
0							40
2						62	35
4				172	106	69	55
6			172	160	110	80	70
8			225	167	128	105	97
10	334	300	238	192	159	140	134

SUMMARY

The author begins by presenting the advantages of putting to avail the three dimensionality in the structural behaviour of a shell, by giving it a double curved shape, so as to obtain an almost exclusively compressive state of stress. He then introduces the notion of funicular surface, a generalization of the funicular curve to the three dimensions.

A mathematical basis is given for an analytical approach to the problem but owing to its complexity, it is only sketched.

It is shown that the problem is very easy to solve by experimental means, the state of stress of the funicular surface being likewise calculated by a quick method, whatever the shape obtained.

The method expounded is then applied to the design of an 80 m high dam.

ZUSAMMENFASSUNG

Der Verfasser weist in erster Linie auf die Zweckmässigkeit der Ausnützung dreier Dimensionen beim Entwurf einer Schale hin. Es soll dieser eine doppelte Krümmung gegeben werden, so dass die Eigenspannungen fast auschliesslich und in allen Richtungen Druckspannungen sind. Dann wird der Begriff «Seilfläche», eine Erweiterung der Seilkurven auf drei Dimensionen, dargelegt.

Der Verfasser erörtert eine mathematische Grundlage zur analytischen Betrachtung dieser Frage, die aber wegen ihrer Komplexität nur leicht skizziert wird.

Es wird die Möglichkeit gezeigt, wie man das Problem experimentell leicht lösen kann, wobei auch der Spannungszustand in der Seilfläche ungeachtet der gefundenen Form rasch festzustellen ist.

Die beschriebene Methode wird dann angewendet zur Berechnung einer 80 m hohen Staumauer.

RESUMO

O autor começa por apresentar a vantagem de se tirar partido das três dimensões no comportamento estrutural duma cúpula dando-lhe dupla curvatura por forma que o estado de tensão seja quase exclusivamente de compressão em todas as direcções. Introduz em seguida a noção de superfície funicular, generalização a 3 dimensões das linhas funiculares.

Apresenta uma base matemática para o tratamento analítico deste problema mas, dada a sua complexidade fica apenas esboçada.

Seguidamente mostra a possibilidade de resolver aquele problema com grande simplicidade por via experimental podendo também calcular-se o estado de tensão na superfície funicular por meio dum método rápido, qualquer que seja a forma obtida.

O método é aplicado a título de exemplo no dimensionamento duma barragem de 80 m de altura.

RÉSUMÉ

L'auteur présente d'abord les avantages que l'on peut avoir à tirer parti des trois dimensions dans le comportement structural d'une coupole, en lui donnant une forme à double courbure de façon à obtenir presque exclusivement des contraintes de compression. Il introduit ensuite la notion de surface funiculaire, généralisation des courbes funiculaires aux trois dimensions.

Il présente une base mathématique permettant de traiter analytiquement le problème, mais, étant donné sa complexité, cette méthode n'est qu' ébauchée.

Il montre ensuite la possibilité de résoudre ce problème très aisément par voie expérimentale, la contrainte à la surface funiculaire pouvant être également calculée au moyen d'une méthode rapide, quelle que soit la forme obtenue.

À titre d'exemple la méthode presentée est appliquée au calcul d'un barrage de 80 m de hauteur.

IIa3

Statischen Behandlung von schiefen Platten

Ensaios estáticos de placas oblíquas

Essais statiques de plaques obliques

Statical tests of skew plates

DR. ING H. VOGT
Eckernförde

Der heutige Verkehr erfordert eine gerade Führung der Verkehrswege auch bei Unter- und Überführungen. Die meisten Brücken, insbesondere fast alle kleineren, müssen daher als schiefe Brücken erstellt werden. Bei vielen dieser Brücken wird das Tragsystem durch eine schiefe Platte über ein Feld oder über mehrere Felder durchlaufend gebildet. Die Frage nach dem Tragverhalten schiefer Platten ist daher für den Brückenbau von grösster Wichtigkeit.

In der letzten Zeit hatte ich Gelegenheit, mehrere schiefe Plattenbrücken zu bearbeiten. Die auftretenden Momente wurden mit Hilfe von Modellversuchen und zwar durch Krümmungsmessungen an Modellen aus Kunststoffplatten [1] bestimmt. Diese Methode der modellmässigen Ermittlung der Momente hat sich bei dieser Bauwerksart bewährt. Durch vergleichende Betrachtungen der einzelnen Untersuchungen in Verbindung mit den vorliegenden theoretischen Untersuchungen konnten wertvolle Erkenntnisse zusammengestellt werden. An dieser Stelle kann ich natürlich die Frage nicht erschöpfend behandeln, sondern kann nur ein ganz kleines Bild von dem umfangreichen Material bringen. Im übrigen weise ich auf die in Kürze erscheinenden Abhandlungen hin.

Es zeigt sich, dass es möglich ist, die Momente, die Momentenrichtungen, die Form der Momentenflächen, sowie die Auflagerkräfte einer schiefen Einfeldplatte mit der für die Praxis erforderlichen Genauigkeit abzuschätzen. Modellversuche für normale, d. h. nicht gleichzeitig gekrümmte schiefe Einfeldplatten sind daher nicht mehr erforderlich.

Die Momente einer schiefen Einfeldplatte können nach den Momenten einer entsprechenden rechtwinkligen Vergleichsplatte berechnet werden. In Bild 1 sind als Beispiel einige Beziehungen dargestellt. Die Beiwerte β und γ sind von dem Verhältnis b/l und der Schiefe φ abhängig und sind bereits in einer Abhandlung in der Zeitschrift Beton- und Stahlbetonbau 1955 [2] veröffentlicht. Die Richtung der Hauptmomente einer schiefen Platte kann für den Bereich der Plattenmitte in erster Annäherung in einer mittleren Richtung zwischen der Richtung des freien Randes und einer Senkrechten auf das Widerlager angenommen werden.

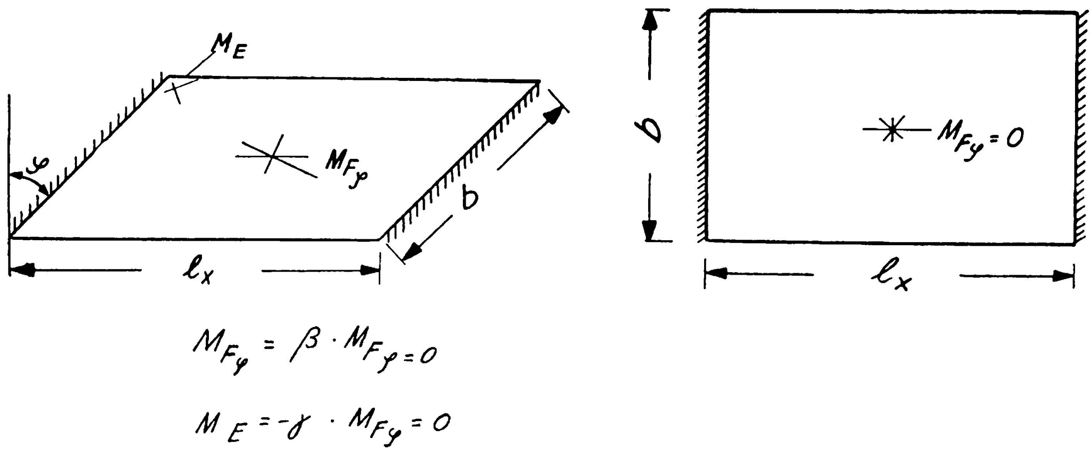

BILD. 1

Aber nicht nur die Momente, sondern auch die Gestalt der Momentenfläche einer schiefen Platte ändert sich gegenüber derjenigen einer rechtwinkligen. Es tritt eine Verschiebung des maximalen Momentenpunktes zur stumpfen Ecke hin auf. Bild 2 und Bild 3 zeigen diese Verschiebung. Der Beiwert «u» ist nur von der Schiefe abhängig. Die

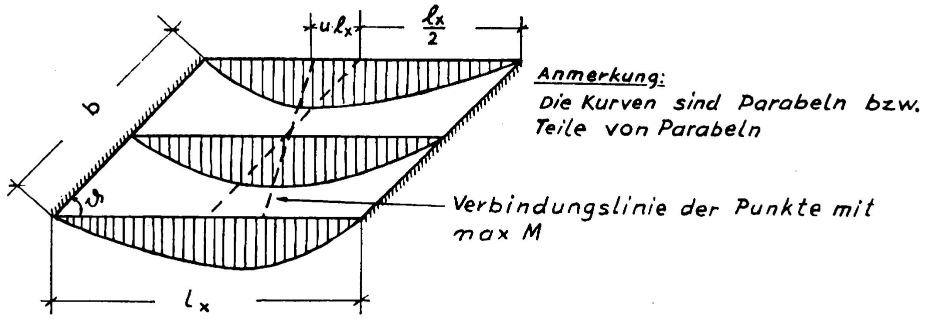

BILD. 2. Momente in Tragrichtung durch ständige Last

grössten Abweichungen gegenüber den Momenten einer rechtwinkligen Platte treten jedoch auf für die Momente quer zur Tragrichtung. Die typischen Formen der Momentenlinien gehen aus Bild 4 hervor. Die Grösse und das Vorzeichen der Momente für den Schnitt c-c ist von der Schiefe und dem Verhältnis b/l abhängig. Bei breiten Platten können die Momente positiv werden. Schon bei verhältnismässig geringer Schiefe kann das negative Moment in der stumpfen Ecke grösser als das maximale Feldmoment werden.

Was die Berechnung der Auflagerkräfte anbelangt, so lassen sich auch hier einfache Beziehungen ableiten, so dass sie für eine schiefe Einfeldbrücke leicht ermittelt werden können.

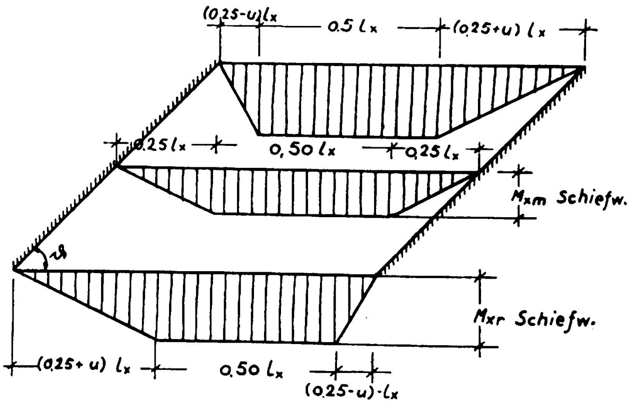

BILD. 3. Momente in Tragrichtung durch Verkehrslast

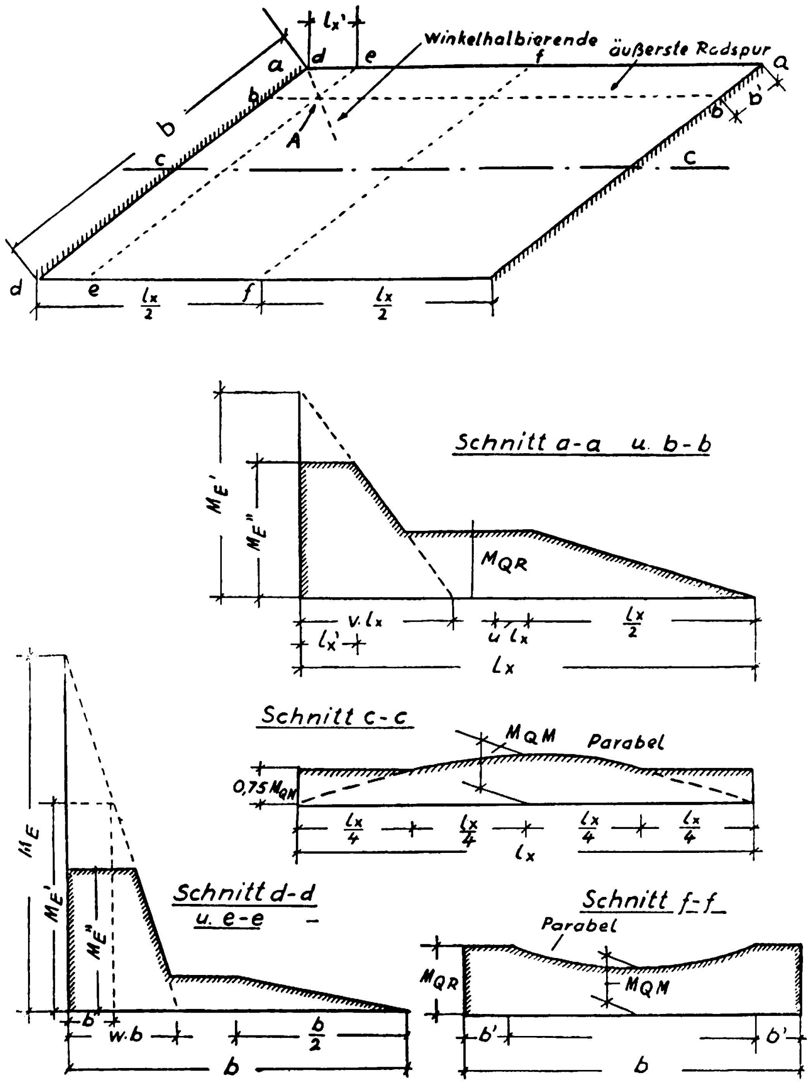

BILD. 4. Grösse und Verteilung der Momente quer zur Tragrichtung

Bei schiefen Plattenstreifen über mehrere Felder werden die auftretenden Fragen natürlich bedeutend schwieriger. Auch hier konnten jedoch eine Reihe wichtiger Erkenntnisse gesammelt werden. Leider sind die Unterlagen noch zu lückenhaft, um ebenso wie bei schiefen Einfeldplatten ein Berechnungsschema anzugeben. Bei schiefen Platten über mehreren Feldern sind daher Modellversuche erforderlich, wenn nicht Modellversuche von Brücken mit ähnlicher Schiefe und ähnlichen Stützweitenverhältnissen vorliegen, die ein Interpolieren gestatten.

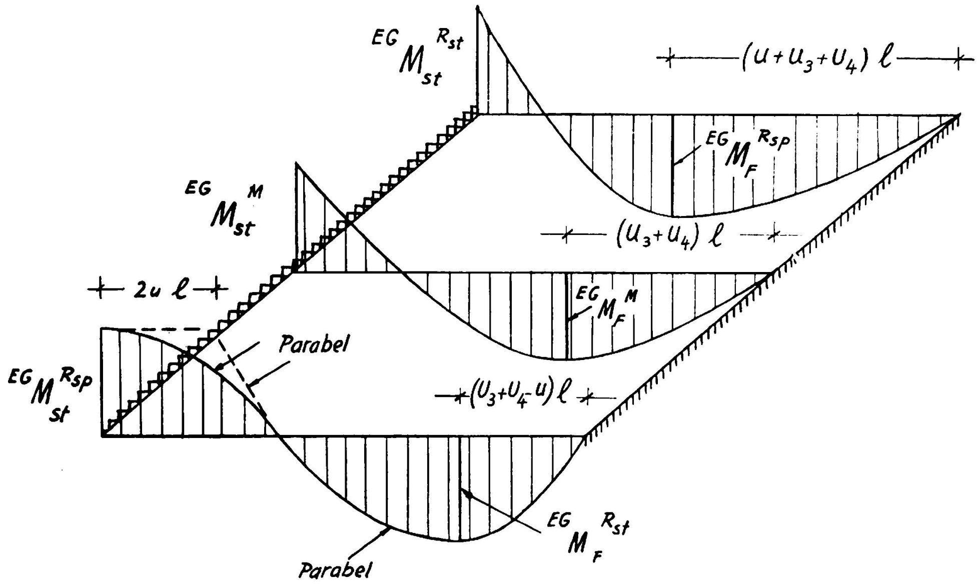

BILD. 5. Momente in Tragrichtung durch ständige Lasten

Als wichtigste Erkenntnis ergab sich, dass das Problem der Durchlaufwirkung und das Problem der Schiefwinkligkeit nicht getrennt behandelt werden können. Die Durchlaufwirkung ist von der Grösse der Schiefwinkligkeit abhängig. Bei schiefwinkligen Systemen geht je nach

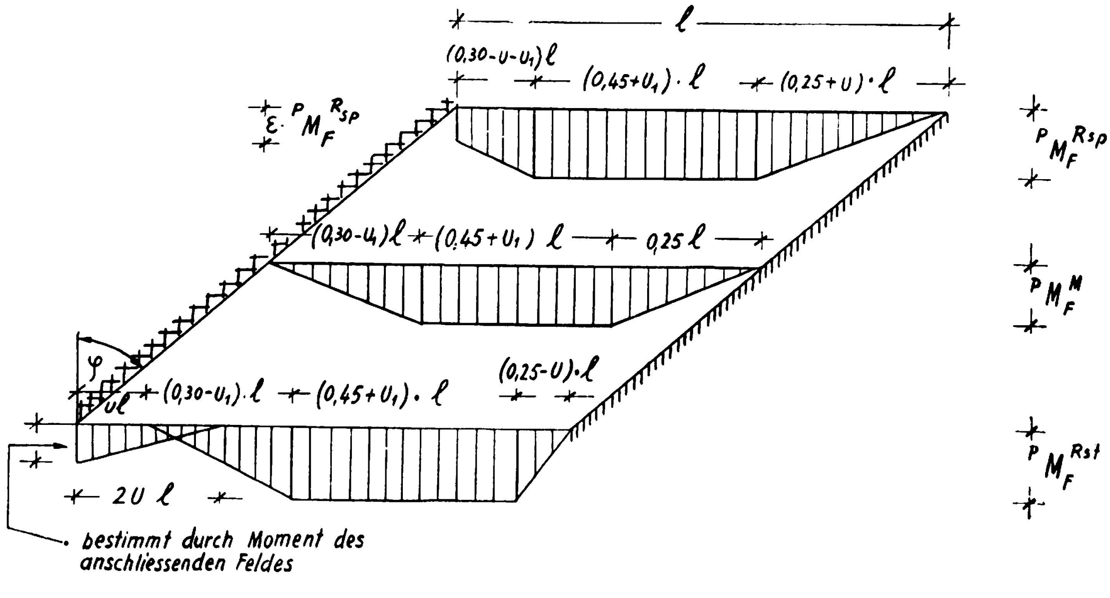

BILD. 6. Positive Momente in Tragrichtung durch Verkehrslast

dem Grad der Schiefe ein Teil der Durchlaufwirkung verloren. Das bedeutet insbesondere für den Fall Eigengewicht, dass die Stützmomente kleiner und die Feldmomente grösser werden.

Für Verkehrslast sind die Verhältnisse noch etwas undurchsichtiger. Man hat aus den bisher vorliegenden Ergebnissen den Eindruck, dass das Verhältnis der extremen Stütz- und Feldmomente vom Winkel unabhängig ist, dagegen jedoch vom Stützweitenverhältnis abhängig ist. Der Winkel macht sich in der Grösse der Momente bemerkbar. Bei den Feldmomenten macht sich mit zunehmender Schiefe der Verlust an Durch-

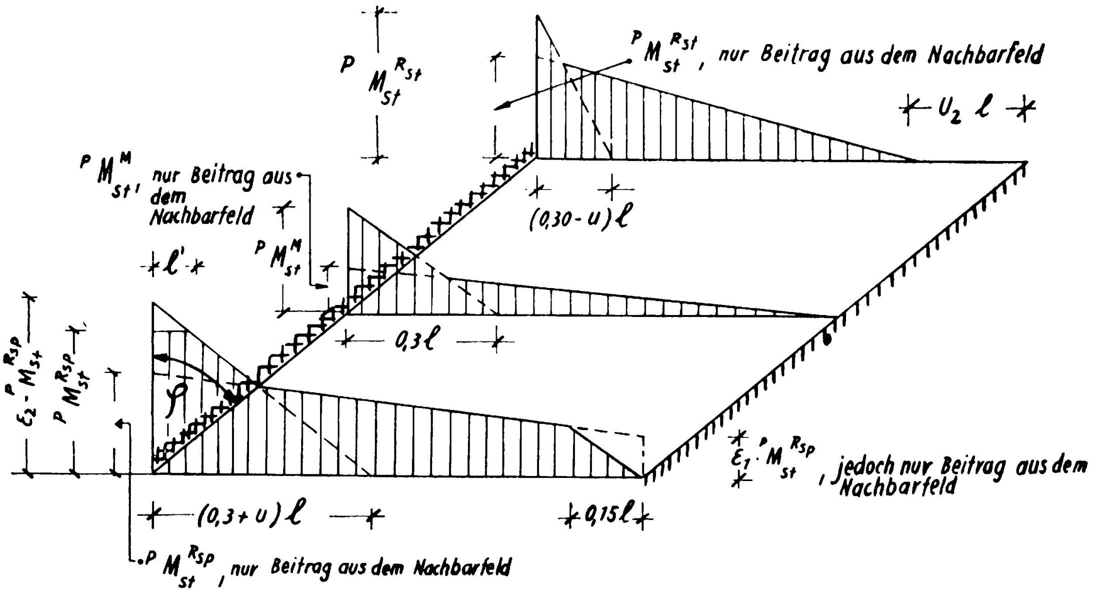

BILD. 7. Negative Momente in Tragrichtung durch Verkehrslast

laufwirkung bemerkbar. Die extremen Feldmomente werden daher grösser als erwartet. Bei den Stützmomenten macht sich die grössere Quersteifigkeit bemerkbar, so dass auch die Stützmomente grösser werden als erwartet.

Auch die Form der Momentenlinien zeigen erhebliche Abweichungen gegenüber den bekannten Formen bei rechtwinkligen Systemen. Als Beispiel sollen hier 3 typische Momentenbilder für ein Endfeld gezeigt werden. (Bild 5, 6, 7).

Die negativen Quermomente am Rande bei durchlaufenden schiefen Platten sind nicht wie bei Einfeldplatten vom positiven Feldmoment abhängig, sondern von der absoluten Summe des Stütz- und Feldmomentes in der Tragrichtung.

LITERATUR

1. VOGT — *Die statische Behandlung schiefwinkliger Brücken.* Der Ingenieur 1955, H. 8.
2. VOGT — *Das statische Verhalten von zweiseitig aufgelagerten schiefwinkligen Einfeldplatten.* Beton- und Stahlbetonbau 1955, H. 11.

ZUSAMMENFASSUNG

Es wird über Erfahrungen bei der statischen Behandlung der für den Brückenbau wichtigen schiefen Platten mitgeteilt. Zweckmässige Untersuchungsmethoden werden genannt. Für den Fall der zweiseitig aufgelagerten schiefen Platten werden Grenzlinien für die Momente in und quer zur Tragrichtung angegeben. Auf typische Besonderheiten des Tragverhaltens durchlaufender Plattenstreifen mit zwei freien Rändern wird hingewiesen.

RESUMO

Descrevem-se ensaios estáticos de placas oblíquas aplicadas na construção de pontes. Indicam-se as envolventes dos momentos, transversal e paralelamente à portada, para o caso de placas oblíquas apoiadas em dois lados. Descrevem-se ainda particularidades típicas de comportamento das placas contínuas com dois lados livres.

RÉSUMÉ

L'auteur décrit des essais statiques de plaques obliques appliquées à la construction de ponts. Il donne les enveloppes des moments parallèlement et transversalement à la portée dans le cas de plaques obliques appuyées sur deux côtés. Il décrit également, des particularités typiques de comportement de plaques continues à deux bords libres.

SUMMARY

Statical tests of skew plates for bridge structures are described. Enveloping curves are given for the bending moments parallel and tranverse to the span, for skew plates supported along two edges. Typical cases of behaviour of continuous plates with two free edges are also described

II a 4

Der Einfluss von biege- und torsionssteifen Randträgern bei Plattenbrücken

Influência dos reforços laterais de torsão e flexão nas pontes-laje

Influence des raidisseurs latéraux de torsion et flexion dans les ponts-dalle

Influence of flexural and torsional edge stiffeners in plate bridges

DR. ING. B. GILG
Elektro-Watt
Zürich

Eine Rechteckplatte von der Dicke h sei längs zwei gegenüberliegenden Rändern im Abstand l frei drehbar gelagert und längs den beiden andern Randern, deren Abstand b beträgt, durch Träger verstärkt. Die Randträgeraxen liegen im Abstand s unter der Plattenmittelfläche. Sämtliche äusseren Lasten greifen an der Platte an, welche einem kombinierten Biege- und Membranspannungszustand unterliegt, während die Verstärkungsträger nur durch die an den entsprechenden Rändern auftretenden Plattenschnittkräfte beansprucht werden. Nach der Elastizitätstheorie gehorcht die Platte den beiden als Platten- und Scheibengleichung bekannten partiellen Differentialgleichungen 4. Ordnung (1). Für den Fall einer gleichmässig belasteten Platte mit gleichartigen Randträgern an den beiden verstärkten Rändern wurden die Schnittkräfte in Funktion der folgenden Parameter zusammengestellt:

λ = Verhältnis der Plattenspannweite zur Plattenbreite.
ε = Verhältnis des Axabstandes der Träger von der Plattenmittelfläche zur Plattendicke.
φ = Verhältnis der Plattenquerschnittsfläche zu derjenigen des Trägers.

---

(1) vgl. Sch. Bauzeitg., 1953, S. 704 ff

n = Verhältnis der Plattenbiegesteifigkeit zur vertikalen Trägerbiegesteifigkeit.
i = Verhältnis der Trägertorsionsteifigkeit zur vertikalen Trägerbiegesteifigkeit.

Der Einfluss der horizontalen Biegesteifigkeit des Trägers ist vernachlässigbar klein. Es werden nur die Werte für i = o und ∞ wiedergegeben, wobei aber die folgende Zahlentabelle erlaubt, bei gegebenem n und λ diejenige Zahl für i zu ermitteln, bei welcher die Schnittkraft den Mittelwert zwischen den beiden oben erwähnten Extremen annimmt:

n	λ = 0,5	1,0	2,0
1/3	i = 0,10	0,18	0,4
1	0,30	0,54	1,2
3	0,9	1,6	3,4

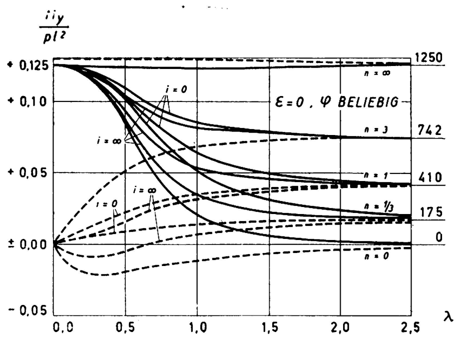

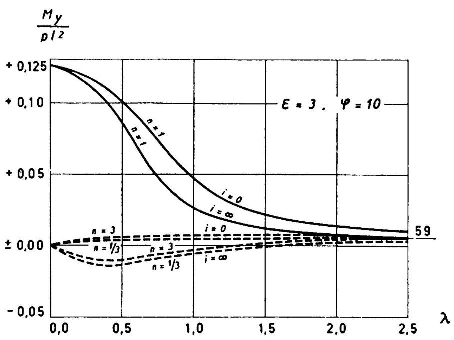

——— PLATTENMITTE

- - - - - PLATTENRAND

$\lambda = \frac{l}{b}$

$\varepsilon = \frac{s}{h}$

$\varphi = \frac{(EF)_{Pl}}{(EF)_R}$

$n = \frac{b \cdot D}{(EJ_x)}$

$i = \frac{(GJ_p)}{(EJ_x)}$

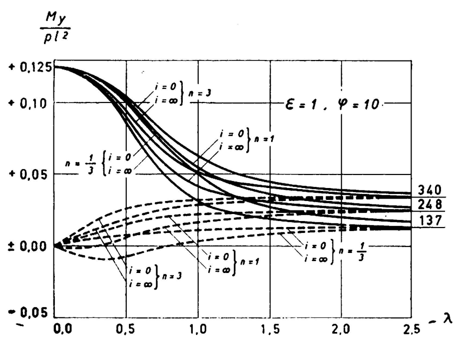

λ		0,5				1,0				2,0				∞				
ε		1		3		1		3		1		3		1		3		
φ		3	30	3	30	3	30	3	30	3	30	3	30	3	30	3	30	
$n = \frac{1}{3}$	$i = 0$	1005	1007	998	1002	488	506	446	473	179	221	106	161	104	158	25	90	$\frac{M_y}{pl^2} \cdot 10^4$ IN DER MITTE
	$i = \infty$	867	872	848	858	303	331	234	279	132	180	49	112					
$n = 1$	$i = 0$	1019	1027	999	1006	533	599	448	494	234	374	109	195	159	329	26	128	
	$i = \infty$	898	917	852	870	373	473	238	313	195	351	52	151					
$n = 3$	$i = 0$	1032	1056	999	1010	566	711	449	506	270	543	110	214	193	514	26	148	
	$i = \infty$	927	975	853	877	424	632	240	332	235	536	53	172					
$n = \frac{1}{3}$	$i = 0$	76	80	27	48	99	128	29	74	106	153	27	87	104	158	25	90	$\frac{M_y}{pl^2} \cdot 10^4$ AM RAND
	$i = \infty$	-78	-63	-146	-113	18	56	-73	-14	82	132	-4	61					
$n = 1$	$i = 0$	150	186	34	75	171	280	33	109	167	321	12	126	159	329	26	128	
	$i = \infty$	39	96	-136	-71	108	241	-68	31	148	311	-2	101					
$n = 3$	$i = 0$	216	338	37	91	224	460	34	128	206	507	30	146	193	514	26	148	
	$i = \infty$	142	302	-131	-46	174	451	-66	56	189	506	-1	174					

FIG. 1. Zeigt die Längsmomente pro Breiteneinheit im Plattenmittelpunkt und im Mittelpunkt des Plattenrandes

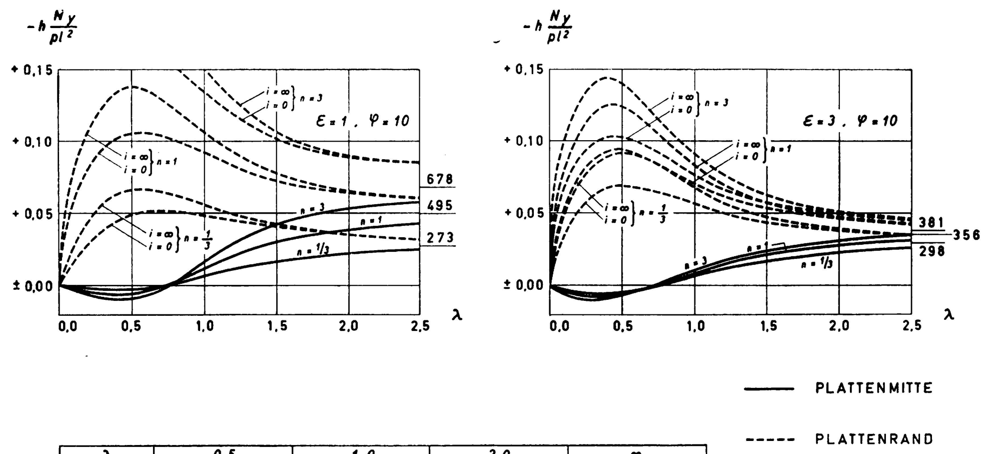

λ		0,5				1,0				2,0				∞				
ε		1		3		1		3		1		3		1		3		
φ		3	30	3	30	3	30	3	30	3	30	3	30	3	30	3	30	
$n = \frac{1}{3}$	i = 0	-33	-14	-39	-25	87	26	78	47	357	91	273	156	502	119	358	202	IN DER MITTE $-h\frac{N_y}{pl^2}\cdot 10^4$
	i = ∞	-45	-19	-54	-34	103	32	94	55	372	93	286	165					
n = 1	i = 0	-67	-32	-49	-39	147	58	90	68	565	192	302	224	764	247	390	287	
	i = ∞	-88	-42	-67	-52	175	66	107	80	587	197	316	233					
n = 3	i = 0	-101	-59	-54	-47	199	96	94	81	700	304	312	261	926	385	401	334	
	i = ∞	-130	-72	-73	-64	229	106	113	95	724	307	327	271					
$n = \frac{1}{3}$	i = 0	650	276	790	504	759	229	674	399	613	154	462	263	502	119	358	202	AM RAND $-h\frac{N_y}{pl^2}\cdot 10^4$
	i = ∞	674	372	1083	687	892	267	802	470	632	157	477	271					
n = 1	i = 0	1348	644	984	775	1304	497	766	581	962	322	507	376	764	247	390	287	
	i = ∞	1694	835	1348	1045	1508	562	910	679	986	326	524	385					
n = 3	i = 0	1955	1165	1065	942	1708	817	802	685	1184	508	524	438	926	385	401	334	
	i = ∞	2444	1434	1458	1263	1954	891	952	797	1212	508	540	448					

$\lambda = \frac{l}{b}$

$\varepsilon = \frac{s}{h}$

$\varphi = \frac{(EF)_{Pl}}{(EF)_R}$

$n = \frac{b \cdot D}{(EJ_x)}$

$i = \frac{(GJ_p)}{l\,\cdot}$

FIG. 2. Zeigt die mit der Plattendicke multiplizierten Längsnormalkräfte pro Breiteneinheit in analoger Lage wie Fig. 1 (N+ = Zug)

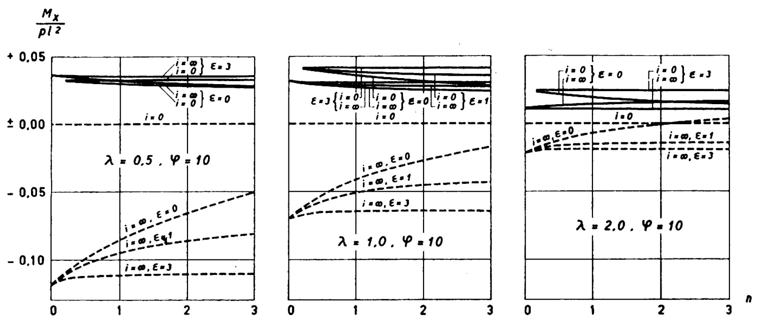

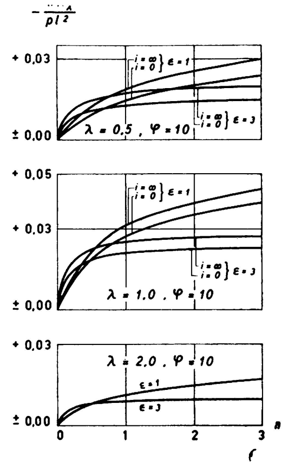

λ	0,5				1,0				2,0				
ε	1		3		1		3		1		3		
φ	3	30	3	30	3	30	3	30	3	30	3	30	
$n = \frac{1}{3}$, $i = 0$	322	321	326	324	406	400	421	411	233	227	244	236	$\frac{M_x}{pl^2} \cdot 10^4$ IN DER MITTE
$n = \frac{1}{3}$, $i = \infty$	349	348	357	353	300	297	307	302	113	117	107	112	
$n = 1$, $i = 0$	315	310	325	321	396	368	420	404	225	203	244	231	
$n = 1$, $i = \infty$	338	330	356	349	293	282	307	299	118	130	107	115	
$n = 3$, $i = 0$	308	295	325	319	380	330	420	400	219	177	244	228	
$n = 3$, $i = \infty$	326	307	353	346	287	265	306	297	122	144	107	116	
$n = \frac{1}{3}$, $i = \infty$	-1080	-1068	-1149	-1115	-612	-587	-673	-632	-174	-158	-202	-181	$\frac{M_x}{pl^2} \cdot 10^4$ AM RAND
$n = 1$, $i = \infty$	-979	-916	-1139	-1076	-552	-463	-669	-604	-153	-100	-201	-167	
$n = 3$, $i = \infty$	-870	-718	-1134	-1052	-507	-325	-667	-588	-141	-38	-201	-160	
$n = \frac{1}{3}$, $i = 0$	92	38	109	70	222	68	199	118	118	24	89	51	$-\frac{hN_x}{pl^2} \cdot 10^4$ IN DER MITTE
$n = \frac{1}{3}$, $i = \infty$	125	51	150	95	262	79	238	140	121	30	91	52	
$n = 1$, $i = 0$	186	89	136	108	383	148	227	173	185	62	97	72	
$n = 1$, $i = \infty$	245	116	186	145	445	168	271	203	189	62	100	73	
$n = 3$, $i = 0$	280	162	148	131	505	244	238	204	227	97	100	84	
$n = 3$, $i = \infty$	361	200	203	176	580	267	284	239	232	97	103	85	

——— PLATTENMITTE

- - - - - PLATTENRAND

$\lambda = \frac{l}{b}$

$\varepsilon = \frac{s}{h}$

$\varphi = \frac{(EF)_{Pl}}{(EF)_R}$

$n = \frac{b \cdot D}{(EJ_x)}$

$i = \frac{(GJ_p)}{(EJ_x)}$

FIG. 3. Zeigt die Quermomente und -Normalkräfte pro Breiteneinheit in den analogen Punkten wie Fig. 1 und 2

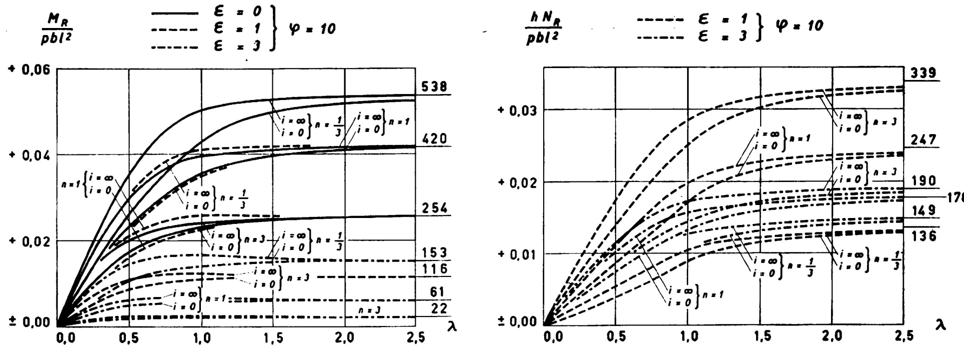

λ		0,5				1,0				2,0				∞				
ε		1		3		1		3		1		3		1		3		
φ		3	30	3	30	3	30	3	30	3	30	3	30	3	30	3	30	
$n = \frac{1}{3}$	i = 0	216	245	84	151	304	394	90	229	328	469	82	269	322	487	76	277	$\frac{M_R}{pbl^2} \cdot 10^4$ IM TRÄGER
	i = ∞	298	330	116	206	359	461	108	271	338	486	86	279					
n = 1	i = 0	153	191	35	77	175	287	34	111	172	329	30	128	163	337	28	131	
	i = ∞	201	249	48	103	202	325	40	131	176	337	31	133					
n = 3	i = 0	74	115	13	31	77	158	12	44	71	174	10	50	66	176	10	51	
	i = ∞	96	142	17	42	88	173	14	51	70	175	10	51					
$n = \frac{1}{3}$	i = 0	53	23	65	42	143	43	128	76	221	56	168	96	251	60	179	101	$\frac{hN_R}{pbl^2} \cdot 10^4$ IM TRÄGER
	i = ∞	68	31	89	57	169	51	153	90	229	58	175	100					
n = 1	i = 0	106	53	81	64	247	95	146	111	349	118	186	137	382	124	195	143	
	i = ∞	136	69	111	86	286	107	175	131	360	120	193	142					
n = 3	i = 0	165	96	88	78	325	157	153	131	431	187	192	160	463	192	201	167	
	i = ∞	210	119	121	106	374	171	183	153	444	188	199	166					

$\lambda = \frac{l}{b}$

$\varepsilon = \frac{s}{h}$

$\varphi = \frac{(EF)_{Pl}}{(EF)_R}$

$n = \frac{b \cdot D}{(EJ_x)}$

$i = \frac{(GJ_p)}{(EJ_x)}$

FIG. 4. Zeigt die im Randträgermittelpunkt auftretenden Trägermomente und- Normalkräfte

ZUSAMMENFASSUNG

Die Schnittkräfte in den Hauptpunkten einer durch Randträger versteiften zweiseitig gelagerten Rechteckplatte sowie in den Trägern werden in Abhängigkeit verschiedener geometrischer und elastischer Parameter in Diagrammen und Tabellen zusammengestellt.

RESUMO

O autor apresenta sob forma de diagramas e tabelas, em função de vários parâmetros geométricos e elásticos, os esforços interiores nos pontos principais de uma placa rectangular apoiada em dois lados e reforçada ao longo dos bordos; também indica os esforços interiores nas vigas de reforço.

RÉSUMÉ

L'auteur présente sous forme de diagrammes et de tables, en fonction de plusieurs paramètres géométriques et élastiques, les efforts intérieurs aux points principaux d'une plaque rectangulaire appuyée aux deux extrémités et raidie le long des bords; il présente également les efforts intérieurs dans les poutres de raidissement.

SUMMARY

The author classifies in diagrams and tables, according to different geometric and elastic quantities, the internal forces at the principal points of an edge-stiffened rectangular plate supported at both ends; internal forces in the stiffening beams are also indicated.

Leere Seite
Blank page
Page vide